ICAM

Institute for Computational and
Applied Mechanics

NUMERICAL INVESTIGATION OF FLOW AROUND RECTANGULAR CYLINDERS WITH AND WITHOUT JETS

By

S. N. Tiwari and S. B. Pidugu
Department of Mechanical Engineering
Old Dominion University, Norfolk, VA 23529

NASA Cooperative Agreement NCC1-232 (S. N. Tiwari, P.I.)
NASA Langley Research Center
Hampton, VA 23681

ODU/ICAM Report 99-101
March 1999

FOREWORD

This is a report on the research topic "Aerodynamic Drag Reduction." This work was conducted as part of the research activities of the Institute for Computational and Applied Mechanics (ICAM) which is now a subprogram of the Institute for Scientific and Educational Technology (ISET). Within the guidelines of the research project, special attention was directed to "Numerical Investigation of Flow Around Rectangular Cylinders with and without Jets." The period of performance of the specific research ended December 31, 1998.

The authors would like to extend their sincere appreciation to Dr. T. O. Mohieldin and Mr. V. Kalburgi for their cooperation and helpful discussions during the course of this study. This work, in part, was supported by the NASA Langley Research Center through Cooperative Agreement NCC1-232. The cooperative agreement was monitored by Dr. Samuel E. Massenberg, Director, Office of Education, NASA Langley Research Center, Mail Stop 400.

NUMERICAL INVESTIGATION OF FLOW AROUND RECTANGULAR CYLINDERS WITH AND WITHOUT JETS

By

S. N. Tiwari[1] and S. B. Pidugu[2]

Department of Mechanical Engineering

Old Dominion University, Norfolk, Virginia-23529

SUMMARY

The problem of flow past bluff bodies was studied extensively in the past. The problem of drag reduction is very important in many high speed flow applications. Considerable work has been done in this subject area in case of circular cylinders. The present study attempts to investigate the feasibility of drag reduction on a rectangular cylinder by flow injection by flow injection from the rear stagnation region. The physical problem is modeled as two-dimensional body and numerical analysis is carried out with and without trailing jets. A commercial code is used for this purpose. Unsteady computation is performed in case of rectangular cylinders with no trailing jets where as steady state computation is performed when jet is introduced. It is found that drag can be reduced by introducing jets with small intensity in rear stagnation region of the rectangular cylinders.

---

[1]Eminent Professor/Scholar

[2]Graduate Research Assistant,

TABLE OF CONTENTS

NOMENCLATURE

A	area of the cell; also length of rectangular cylinder
B	height of rectangular cylinder
a	convection/diffusion coefficient
C_p	base pressure coefficient
C_d	drag coefficient
C_l	lift coefficient
C_m	blowing jet momentum coefficient
p	pressure
Re	Reynolds number
S	source
t	time
u	velocity component in x-direction
v	velocity component in y-direction
V	volume of control volume
ρ	density
ϕ	general field property function

Subscript

E,N,W,S	neighboring cell centers (EAST, NORTH, WEST, SOUTH)
e,n,w,s	cell faces (east, north, west, south)

j	jet condition
P	cell center
∞	upstream condition
n	time level
*	guessed value
‘	corrected value

LIST OF TABLES

LIST OF FIGURES

Chapter 1

INTRODUCTION

The problem of flow past bluff bodies is one of the oldest in the fluid mechanics, and it remains one the most important problem due to the complexity of the fluid dynamic phenomena despite their geometrical simplicity. Cylinders of different cross sections such as circular, rectangular and their combinations have been used in the past, due to many practical applications. Various fluid dynamic issues of prime interest and importance in this problem are drag minimization, vortex shedding and aeroelastic instability.

The subject of bluff body flows has recently been receiving a great deal of attention. This is largely because of its importance for energy conservation. For example, road vehicles must now meet more stringent fuel consumption requirements which translate into the need for reduced drag. Large structures such as tall buildings must also be designed so as to minimize convective heat losses. Besides, large structures must be designed so as to avoid potentially disastrous wind induced large amplitude oscillations. This needs knowledge of the vortex shedding characteristics and is also crucial in the design of vortex shedding flowmeter for measuring flow inside closed conduits. Therefore, this field of study is highly desirable.

Roshko[1] extensively conducted wind tunnel experiments to investigate the drag and shedding frequency of two dimensional bluff bodies. A correlation between bluff bodies of different shapes was obtained in order to calculate the drag by combining free streamline theory with experimental results. Bostock and Mair [2] experimentally determined drag and base pressure coefficients around rectangular and D-shaped cylinders for Reynolds number between 0.5×10^5 to 1.6×10^5. For cylinders of D-shaped section, it was shown that the pressure distribution on the

curved surface and drag are considerably affected by the state of boundary layer at the separation point, as for a circular cylinder. Furthermore, they showed empirical correlations for drag based on the known values for the constituent half-bodies are, in general, unsatisfactory. Bearman and Truman [3] measured base pressure coefficient, drag coefficient and Strohaul number of rectangular cylinders for Reynolds number between 2 X 10^4 to 7 X 10^4. It was also demonstrated that the flow around sections is found to be strongly influenced by the percentage of the trailing edge corners. Knauess and John [4] obtained a correlation between Reynolds number and Strauhal number for elliptical cylinders through experiments. A correlation of data on Strouhal number variation with angle of incidence, based on the projected height of the model, is obtained for both square and elliptical models in the range of Reynolds numbers between 300 and 1200. Strouhal numbers of rectangular cylinders have been determined experimentally by Atsushi [5] as a function of Reynolds number (70 - 2 X 10^4) and aspect ratio(1 to 4). They observed, for a certain range of Reynolds number for cylinder with aspect ratio of 2 and 3, flow pattern changes abruptly with a sudden discontinuity in the Strouhal number.

Various numerical investigations have been also conducted on the flow past bluff bodies[6-8]. Clements [6] developed an inviscid model of two dimensional vortex shedding in order to numerically predict flow features behind bluff bodies, form of vortex shedding and Strouhal number. Davis and Moore [7] presented numerical solutions for two dimensional flow about rectangles in infinite domains. The range of Reynolds numbers used was from 100 to 2800. The numerical work was extended to include the effects of confining walls [8].

Many investigators used different shapes of bluff bodies as well as different methods of flow control in order to make their studies useful for practical applications. Jet blowing method near the rear stagnation region is widely used in order to reduce the drag by various investigators

[9,10]. A splitter plate behind the cylinder is a popular technique used by many investigators to reduce the drag [11]. Both methods have advantages and disadvantages. The advantage of using a splitter plates is that no power is required to reduce drag significantly. This can be done easily by placing a plate in the existing system without need of any complicated mechanisms. However, this method is not suitable for cases where rectangular cylinders have non-zero angle of attack. Any mechanism to make splitter plate to adjust its direction in the flow brings additional mechanical complications, thus making the system lose its simplicity. Moreover, it is difficult to control the amount of the effect of the plate. On the other hand, jet blowing method is capable to change direction as well as its strength; and, more importantly, the jet can be actuated only when it is needed without any geometrical change. Particularly, this method is very useful when compressed air is readily available. The present study attempts to investigate the feasibility of drag reduction on a rectangular cylinder by flow injection from the rear stagnation region.

As mentioned earlier, many investigations are limited to flow past circular and rectangular cylinders. Considerable amount of work also has been done by introducing jets as well as splitter plates in the rear stagnation point, in case of circular cylinders. But there is little or no information available on the effect of jet injection from the rear stagnation point of rectangular cylinders on the flow characteristics. The present study is directed to the investigation of the effect of free stream Reynolds number and aspect ratio on the flow past rectangular cylinders with and without jets. Heat transfer aspects are not considered in this study.

Chapter 2

GENERAL FORMULATION

2.1 Physical Model

The physical model, as shown in Fig. 2.1, consists of a rectangular cylinder placed halfway between two channels separated by a distance L. The rectangular shape has known length A and height B. The diameter of the orifice on the rear face of the rectangle is kept at 10 percent of the height of the rectangle when jet injection is considered. The channel length is also sufficiently long in order to exclude the wall end effects that might arise in the computation. The upstream face of the rectangle is located at a distance x_r from the inlet. The problem is limited to two dimensions in order to reduce the computational time and memory requirements. Free stream Reynolds number based on rectangle length is varied from 1×10^4 to 1.25×10^5.

2.2 Numerical Formulation

2.2.1 Governing equations

The two-dimensional time dependent continuity and momentum equations for a Newtonian fluid with constant density and viscosity are given by

Continuity

$$\frac{\partial u}{\partial x} + \frac{\partial v}{\partial y} = 0 \tag{2.1}$$

X-momentum

$$\frac{\partial}{\partial t}(\rho u) + \frac{\partial}{\partial x}(\rho u^2) + \frac{\partial}{\partial y}(\rho uv) = -\frac{\partial p}{\partial x} + \mu\left(\frac{\partial^2 u}{\partial x^2} + \frac{\partial^2 u}{\partial y^2}\right) \tag{2.2}$$

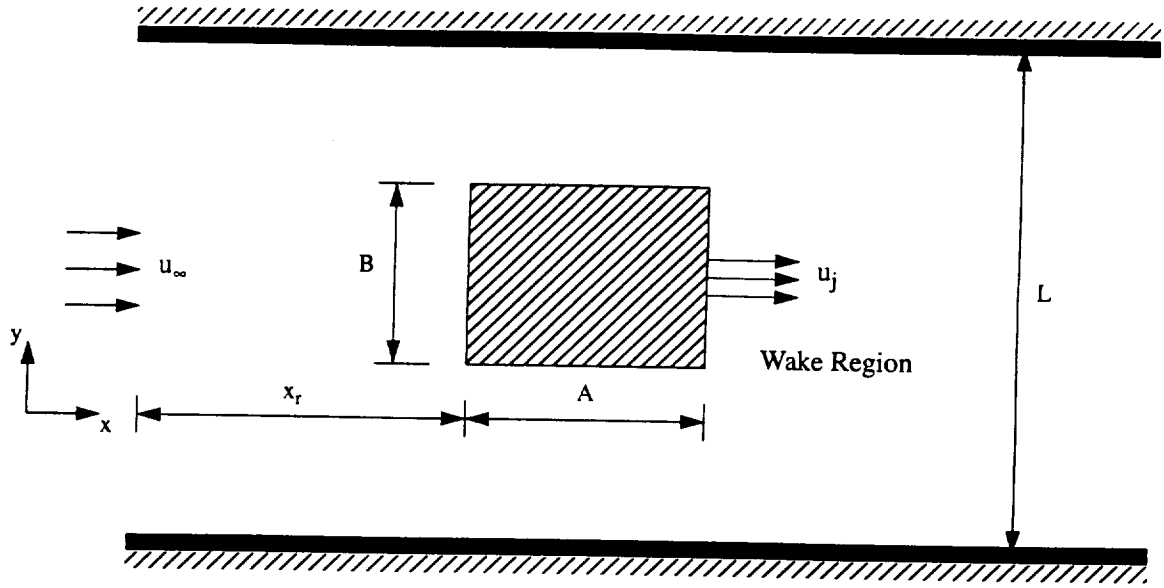

Fig. 2.1 Physical model for two dimensional flow past a rectangle cylinder with jet

Y-momentum

$$\frac{\partial}{\partial t}(\rho v) + \frac{\partial}{\partial x}(\rho uv) + \frac{\partial}{\partial y}(\rho v^2) = -\frac{\partial p}{\partial y} + \mu\left(\frac{\partial^2 v}{\partial x^2} + \frac{\partial^2 v}{\partial y^2}\right) \tag{2.3}$$

Equations (2.1) - (2.3) can be written in a compact form by denoting the dependent variable as ϕ. Thus, the governing differential equations can be expressed in general form as

$$\frac{\partial}{\partial t}(\rho\phi) + \nabla(\rho\vec{v}\phi) = \nabla[\Gamma_\phi(\text{grad}\,\phi)] + S_\phi \tag{2.4}$$

where the corresponding values for ϕ, Γ_ϕ, and S_ϕ are listed in Table 2.1.

2.2.2 Boundary conditions

Boundary conditions required for the physical problem are shown in Fig. 2.2. No slip conditions are imposed on the confining walls as well as on the surface of the cylinder. Neuman conditions are employed at the downstream outlet where gradient of the dependent variable in the normal direction is fixed at zero. Free stream velocity is given at the inlet. When jet is introduced, the fixed velocity is given at the jet slot.

2.2.3 Solution Procedure

Detailed formulations and solution procedures are given in Fluent manual [12,13]. Here, few necessary details on the theory are provided for the analysis of the present problem. The governing equations, Eqs. (2.4), are reduced to finite difference analogs by integration over the computational domain dividing it into number of cells.

Table 2.1 Values of ϕ,Γ_ϕ,S_ϕ in Eq. (2.4)

Equation	ϕ	Γ_ϕ	S_ϕ
mass	1	ρ	0
x-momentum	u	μ	$\frac{\partial P}{\partial x} + S_x$
y-momentum	v	μ	$\frac{\partial P}{\partial y} + S_y$

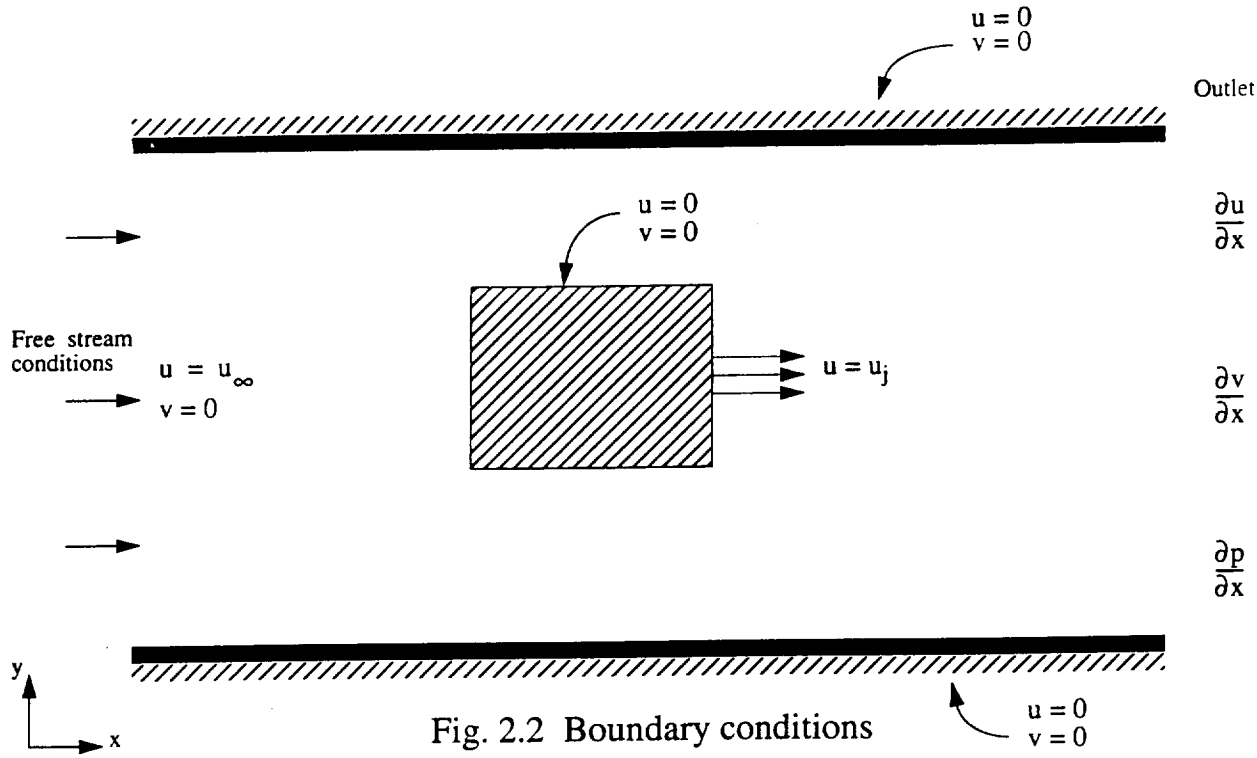

Fig. 2.2 Boundary conditions

Time integration of the transient terms can be descritized as

$$\int_{t}^{t+\Delta t} \frac{\partial}{\partial t}(\rho\phi)dt = (\rho\phi)^{n+1} - (\rho\phi)^{n} \tag{2.5}$$

where n is the time level

Time integration of other terms of Eqs. (2.4) can also be written, in general form, as

$$\int_{t}^{t+\Delta t} \frac{\partial}{\partial t}(\rho u\phi)dt = [f\,(\rho u\phi)^{n+1} + (1-f)\,(\rho u\phi)^{n}]\Delta t \tag{2.6}$$

where f is a factor which determines whether the solution is explicit or implicit. Fluent assumes f =1, which corresponds to the case of fully implicit; hence

$$\int_{t}^{t+\Delta t} \frac{\partial}{\partial t}(\rho u\phi)dt = f\,(\rho u\phi)^{n+1}\Delta t \tag{2.7}$$

Divergence theorem is employed to perform volume integration of the space divided over the control volume as

$$\int_{V} \frac{\partial}{\partial x}(\rho\vec{V}\phi)dV = \int_{A}(\rho\vec{V}\phi)dA \tag{2.8}$$

where V is the volume of the control volume and A is the area of the control surface. After descritizing the integral on the control volume as shown in Fig. 2.3, the surface derivative terms in governing equations become (for example in the x-direction)

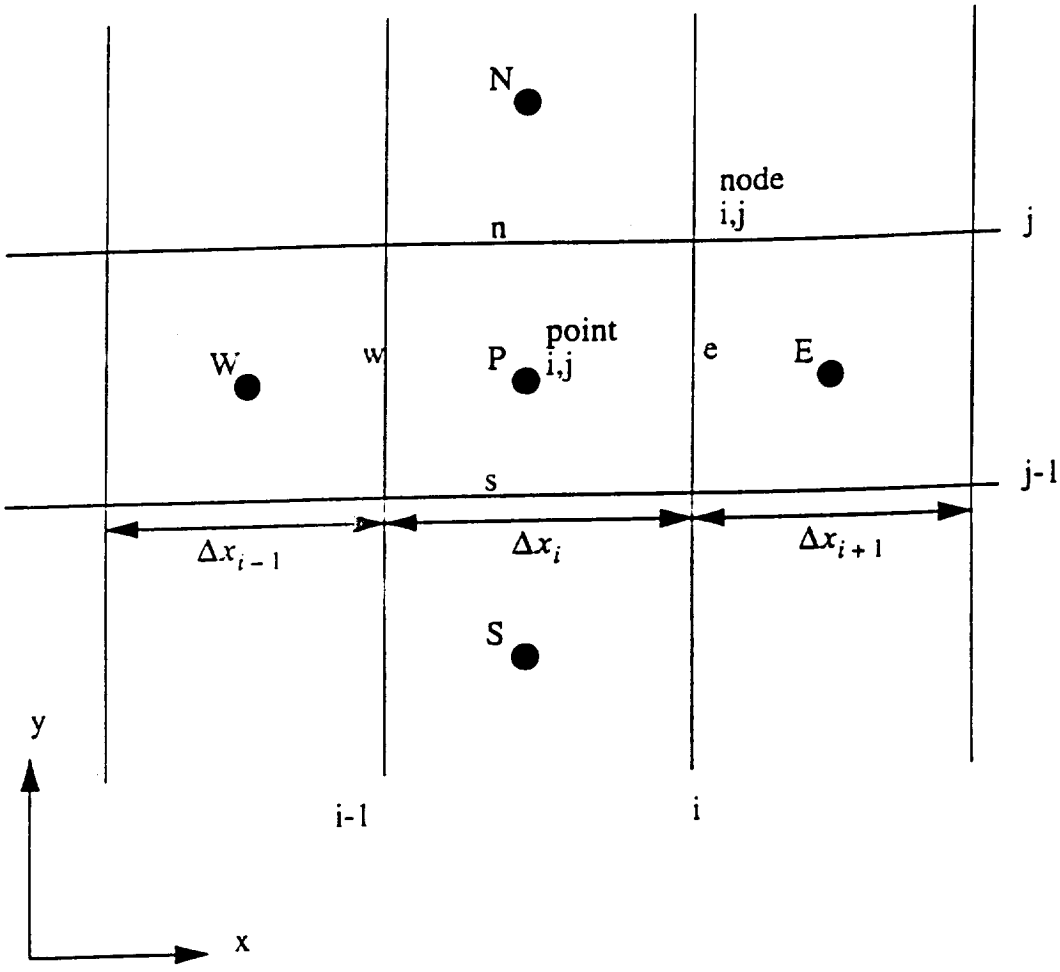

Fig. 2.3 Non-staggered control volume

$$(\rho u\phi A)_c - ((\rho u\phi A)_w + (\rho u\phi A)_n - (\rho u\phi A)_s)$$

$$= \left[\Gamma_\phi \frac{(\phi_e - \phi_p)}{\Delta x} A\right]_e - \left[\Gamma_\phi \frac{(\phi_p - \phi_w)}{\Delta x} A\right]_w$$

$$\left[\Gamma_\phi \frac{(\phi_n - \phi_p)}{\Delta x} A\right]_n - \left[\Gamma_\phi \frac{(\phi_p - \phi_s)}{\Delta x} A\right]_s + S_\phi A \qquad (2.9)$$

where source term S_ϕ can be expressed as $S_\phi = -(p_e - p_w)$

For two dimensional case, we can write complete descritized analog of governing equation as

$$\frac{(\rho\phi V)_p^{n+1} - (\rho\phi V)_p^n}{\Delta t}$$

$$+ (\rho u\phi)_e^{n-1} - (\rho u\phi)_w^{n+1} + (\rho u\phi A)_n^{n+1} - (\rho u\phi A)_s^{n+1}$$

$$= \left[\Gamma_\phi \frac{(\phi_e - \phi_p)}{\Delta x} A\right]_e^{n+1} - \left[\Gamma_\phi \frac{(\phi_p - \phi_w)}{\Delta x} A\right]_w^{n+1}$$

$$+ \left[\Gamma_\phi \frac{(\phi_n - \phi_p)}{\Delta y} A\right]_n^{n+1} - \left[\Gamma_\phi \frac{(\phi_p - \phi_s)}{\Delta y} A\right]_s^{n+1} - S_\phi^{n+1} A \qquad (2.10)$$

By collecting terms with respect to space, Eq. (2.10) can be written in algebraic form as

$$a_p\phi_p = M^{old}\phi_p^{old} + a_e\phi_e + a_w\phi_w + a_n\phi_n + a_s\phi_s + S_\phi \qquad (2.11)$$

where $M^{old} = (\rho V)^{old}$ which corresponds to n-level in time in Eq. (2.11), while other terms are evaluated at (n+1) level in time. Finally, Eq. (2.11) can be written in compact form as

$$a_p\phi_p = \sum_{nb}\phi_{nb}\phi_{nb} + S_\phi + M^{old}\phi_p^{old} \tag{2.12}$$

where subscript nb refers to neighboring points.

The equations are solved using the SIMPLE algorithm which is based on using a relationship between velocity and pressure correction in order to recast the continuity equation in terms of pressure correction calculations.

Using S_ϕ in Eq. (2.12), the momentum equations are expressed as

$$\text{x-direction}: \; a_p u_p = \sum_{nb} a_{nb}u_{nb} + (p_w - p_e)A + (\dot{M}^{old}\phi_p^{old})_x \tag{2.13}$$

$$\text{y-direction}: \; a_p v_p = \sum_{nb} a_{nb}v_{nb} + (p_n - p_s)A + (\dot{M}^{old}\phi_p^{old})_y \tag{2.14}$$

In general, velocities obtained from Eqs. (2.13) and (2.14) do not satisfy the continuity equation until pressure values are substituted in the source term of the equation. To overcome this problem, the continuity equation is used to obtain the correct pressure values. Thus, in turn, correct velocities are obtained which satisfy the continuity equation,. This is the essence of the SIMPLE algorithm.

The SIMPLE algorithm starts with the substitution of a guessed pressure field, p^*, into momentum equations which can be solved to obtain guessed velocity field, u^*. These guessed values are related as

$$u_p = u_p^* + u_p' \tag{2.15}$$

$$v_p = v_p^* + v_p' \tag{2.16}$$

$$p_e = p_e^* + p_e' \tag{2.17}$$

where prime denotes corrected values. Substitutions of Eqs. (2.15)-(2.17) into Eqs. (2.13) and (2.14) with corrected values, yield

$$\text{x-direction}: \quad a_p u_p' = \sum_{nb} a_{nb} u'_{nb} + (p_w - p_e)A \tag{2.18}$$

$$\text{y-direction}: \quad a_p v_p' = \sum_{nb} a_{nb} v'_{nb} + (p_n - p_s)A \tag{2.19}$$

Equations (2.13) and (2.14) are used to relate the pressure and velocity corrections as

$$\text{x-direction}: \quad u_p' = \frac{1}{A_p}(p'_w - p'_e)A \tag{2.20}$$

$$\text{y-direction}: \quad v_p' = \frac{1}{A_p}(p'_n - p'_s)A \tag{2.21}$$

In Eqs. (2.20) and (2.21), the terms containing the neighbor influences are dropped for convenience. However, these terms vanish when convergence is achieved.

To obtain correction terms of pressure, the descritized continuity equation is employed which can be expressed as

$$(\rho uA)_e - (\rho uA)_w + (\rho vA)_n - (\rho vA)_s = 0 \tag{2.22}$$

In Eq. (2.22), u and v are replaced by starred (*) and primed (') values using Eqs. (2.15) and (2.16). Moreover, the primed values are represented by the pressure correction terms through Eqs. (2.20) and (2.21). Finally the pressure correction equation can be expressed as

$$\begin{aligned}
&(\rho u^* A)_e - (\rho u^* A)_w + (\rho v^* A)_n - (\rho v^* A)_s \\
&+(\rho A)_e \frac{1}{(A_p)_e}(p'_p - p'_E) - (\rho A)_w \frac{1}{(A_p)_w}(p'_W - p'_p) \\
&+(\rho A)_n \frac{1}{(A_p)_n}(p'_p - p'_N) - (\rho A)_s \frac{1}{(A_p)_s}(p'_S - p'_p) = 0
\end{aligned} \tag{2.23}$$

The Eq. (2.23) is used for the pressure correction which is then used to compute velocity correction via. Eqs. (2.20) and (2.21). Finally, the velocity and pressure are updated using Eqs. (2.15)-(2.17). The system of implicit equations are solved by using the line Gauss Siedal method.

2.2.4 Time Step

Physical problems which are time dependent should be solved by choosing proper time step in order to capture physical phenomena accurately (time accurate). Since, the Fluent code uses fully implicit scheme, and there is no way to find out the CFL number condition in the Fluent code, several numerical experiments have been conducted to check the effect of the time step on the computations. After several trials, different values of time steps are selected for different inlet velocity conditions.

When the jet is introduced in the wake region, the problem is solved by using the steady state assumption. This assumption is mainly based on the justifications given in the work done by Atsuchi [13]. Steady state assumption reduces the computational time (by several times) as well as large memory requirements to store the data at different time steps.

2.2.5 Grid System

Several grid sizes have been tested to compare the results and performances. A grid size of 115 X 62 is employed for computational purposes as shown in Fig. 2.4. To get the physical phenomena correctly near the surface region, grid points are highly clustered near the wall. When the jet is introduced in the wake region, a more dense grid of size 130 X 71 is employed. In this case, grid is also clustered near the jet mixing region as shown in Fig. 2.5.

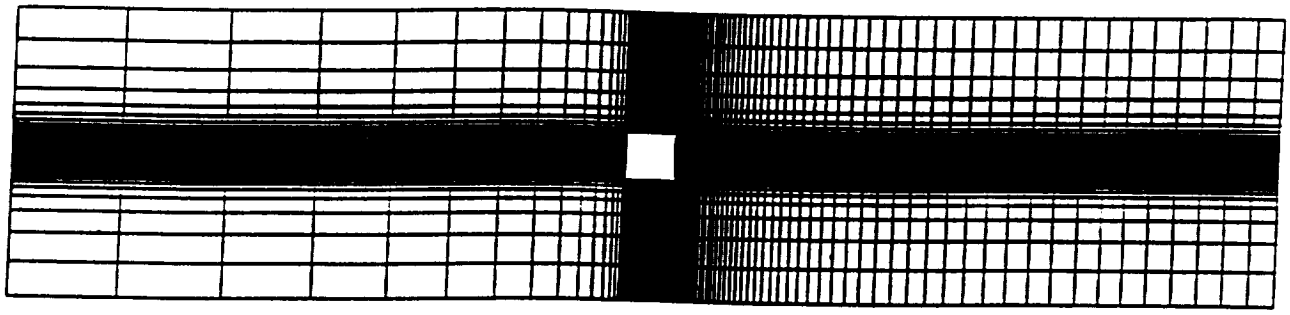

Fig. 2.4a Grid system around a rectangular cylinder without jet

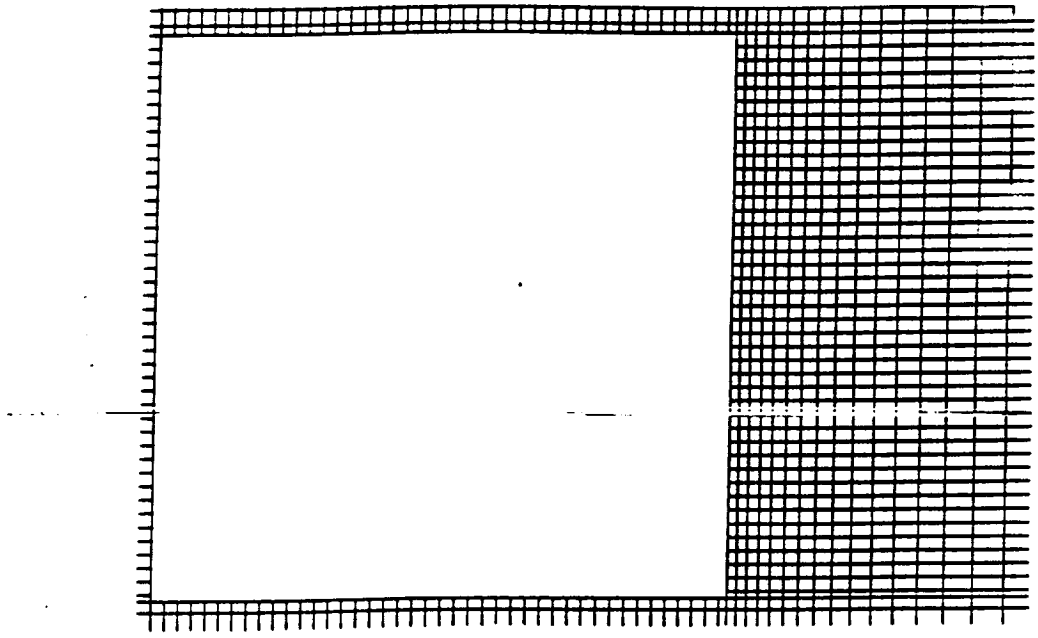

Fig. 2.4b Grid system around a rectangular cylinder without jet (in the vicinity of the wall)

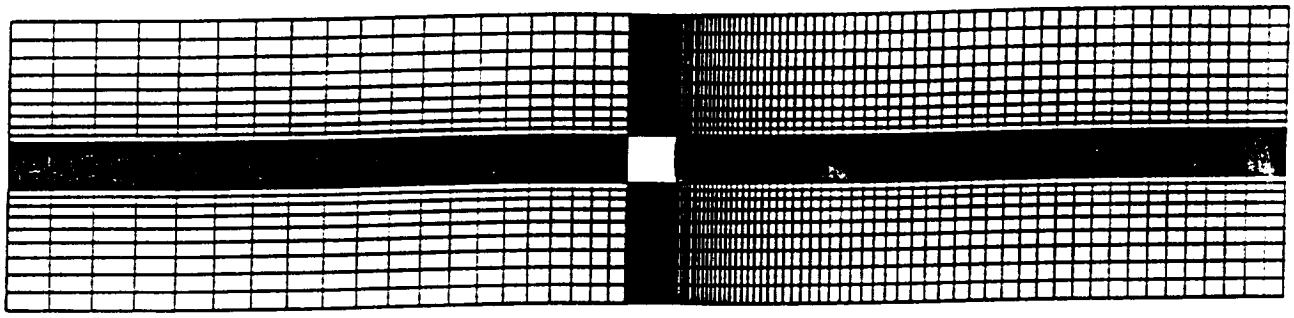

Fig. 2.5a Grid system around a rectangular cylinder with jet

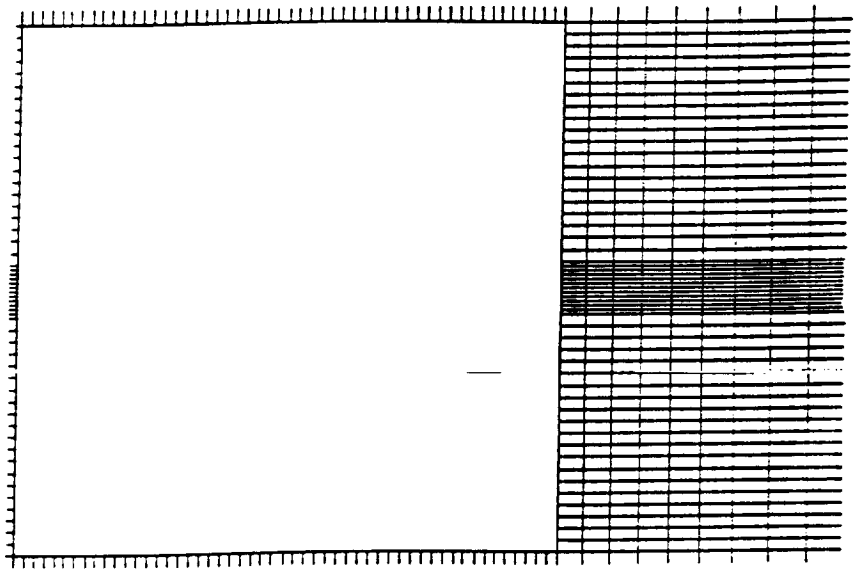

Fig. 2.5b Grid system around a rectangular cylinder with jet (in the vicinity of the wall)

2.3 Important Parameters

Important parameters are presented in this section.

2.3.1 Base pressure coefficient, Cp

$$C_p = \frac{P - P_\infty}{\frac{1}{2}\rho_\infty U^2_\infty}$$

2.3.2 Strouhal number, St

$$St = \frac{f\,h}{U_\infty}$$

where f is the frequency of vortex shedding. The Strouhal number is a very important non-dimensional number for the flow around bluff bodies which shed vortices into the down stream. The variation in the flow pattern can be related to the change in the value of the Strouhal number.

2.3.3 Drag coefficient, Cd

$$C_d = \frac{D}{\frac{1}{2}\rho_\infty U^2_\infty h}$$

2.3.4 Lift coefficient, Cl

$$C_l = \frac{L}{\frac{1}{2}\rho_\infty U^2_\infty d}$$

Here D and L are drag and lift forces.

2.3.5 Jet blowing momentum coefficient, Cm

To evaluate and normalize the strength of the jet, the jet blowing momentum coefficient, C_m, is used as given in [10], i.e.,

$$C_m = \frac{\rho_j d_j u_j^2}{\frac{1}{2}\rho_\infty u_\infty^2 B}$$

In this study, ρ_j and ρ_∞ are same and, therefore, the strength of the jet is normalized with respect to the cylinder height and free stream velocity. Here subscripts ∞ and j represent free stream and jet conditions respectively.

Chapter 3

DISCUSSION OF RESULTS

In this section, first results are presented for the case without jet, followed by the results for the case with jets. As mentioned earlier, complete analysis is carried out using a well known and widely used commercial CFD code, Fluent. In CFD analysis, the need for validating the results by comparing with experimental results or by other means is well established. Many times, this process becomes a very difficult task due to lack of experimental and numerical results. In the present study, results are compared with existing data or with the data obtained using similar physical configurations, but not exactly the same. In the latter case, effort is directed to justify when such comparisons are made.

It is important to note some typical observations regarding flow past circular and rectangular cylinders based on the information available in the literature. One important similarity between these two configurations is the vortex shedding phenomena observed in both cases. The important difference between the two configurations is the point of flow separation. In case of rectangular cylinders, the flow separates at the leading edge, even for very low Reynolds number [5]. The point of flow separation, in case of circular cylinders, is highly dependent on the free stream Reynolds number. The point of separation moves away from the wake and towards the upstream with increase in Reynolds number [14]. These well established observations can be utilized for validating numerical results if necessary.

The Strohaul number, base pressure coefficient, and lift and drag coefficients, are computed for the case with no jets for different free stream Reynolds numbers. Few cases are also considered using different aspect ratios. In the case of situation with jets, drag coefficients are

evaluated for different free stream Reynolds numbers. The effect of introducing a jet on drag is analyzed.

3.1 Case 1: No Jet

Unsteady state computation is carried out when no jet is considered at the rear stagnation region. As mentioned in the previous section, the values of time steps for different inlet conditions (Reynolds numbers) are chosen after several trial tests. The time steps chosen for different Reynolds numbers is listed in the Table 3.1. Free stream Reynolds number is varied from 1 X 10^4 to1.25 X 10^5. Size of the time step decreases with the increase in free stream Reynolds number. The physical reason for this trend is, due to the increase in Reynolds number, the change in flow takes place rapidly. Consequently, a small time step is needed to capture the physical processes more accurately.

The Strouhal number variation with the free stream Reynolds number is listed in the Table 3.2. It is a general practice to numerically compute the Strouhal number based on the fluctuations of pressure or lift coefficient [7]. Here, the Strouhal number is estimated based on the time of one cycle of the pressure fluctuation. Figures 3.1-3.5 show the pressure fluctuation with time for different Reynolds numbers considered in this study. The results were computed on the center point of top edge of the rectangle with aspect ratio equal to unity. From these plots, frequency needed to estimate the Strouhal number is obtained. The results for pressure fluctuation with time for different Reynolds numbers are shown in Fig. 3.6. The frequency of pressure fluctuation increases with the increase in the free stream Reynolds number. The variation of the Strouhal number with the free stream Reynolds number is shown in Fig. 3.7. For the range of the free stream Reynold number used in this study, the value of the Strouhal number remained constant at about 0.12. Atsuchi

Table 3.1 Size of time step for different free stream Re numbers

Reynolds number	1×10^4	2.5×10^4	50×10^4	75×10^4	1.25×10^5
Time step size, in Sec.	0.1	0.05	0.02	0.02	0.01

Table 3.2 Variation of Strouhal number with free stream Re number(AR = 1)

Reynolds number	1×10^4	2.5×10^4	5.0×10^4	7.5×10^4	12.5×10^5
Strouhal number	0.1187	0.1194	0.1179	0.1114	0.1037

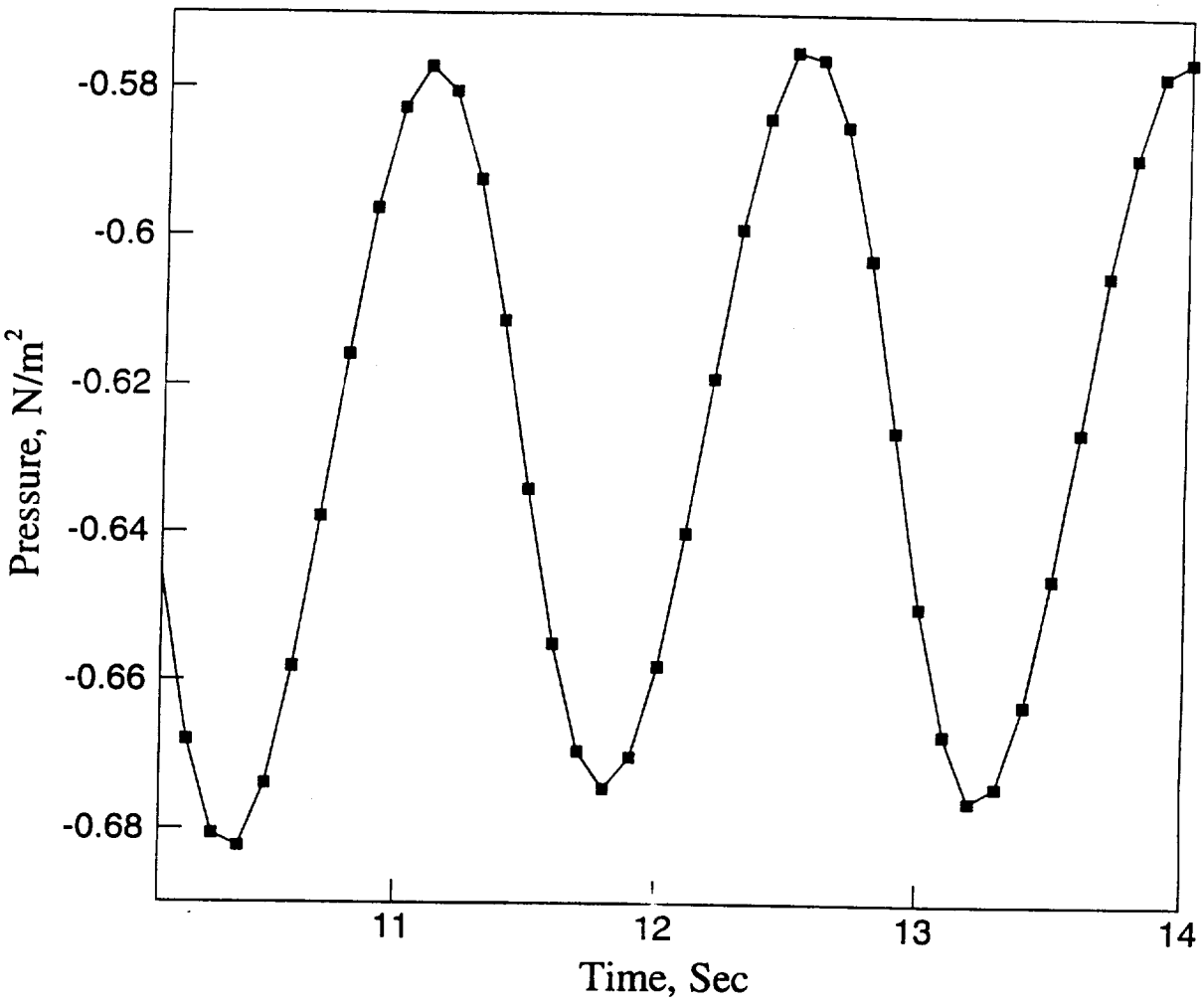

Fig. 3.1 Time history of pressure (Re = 1 X 10^4)

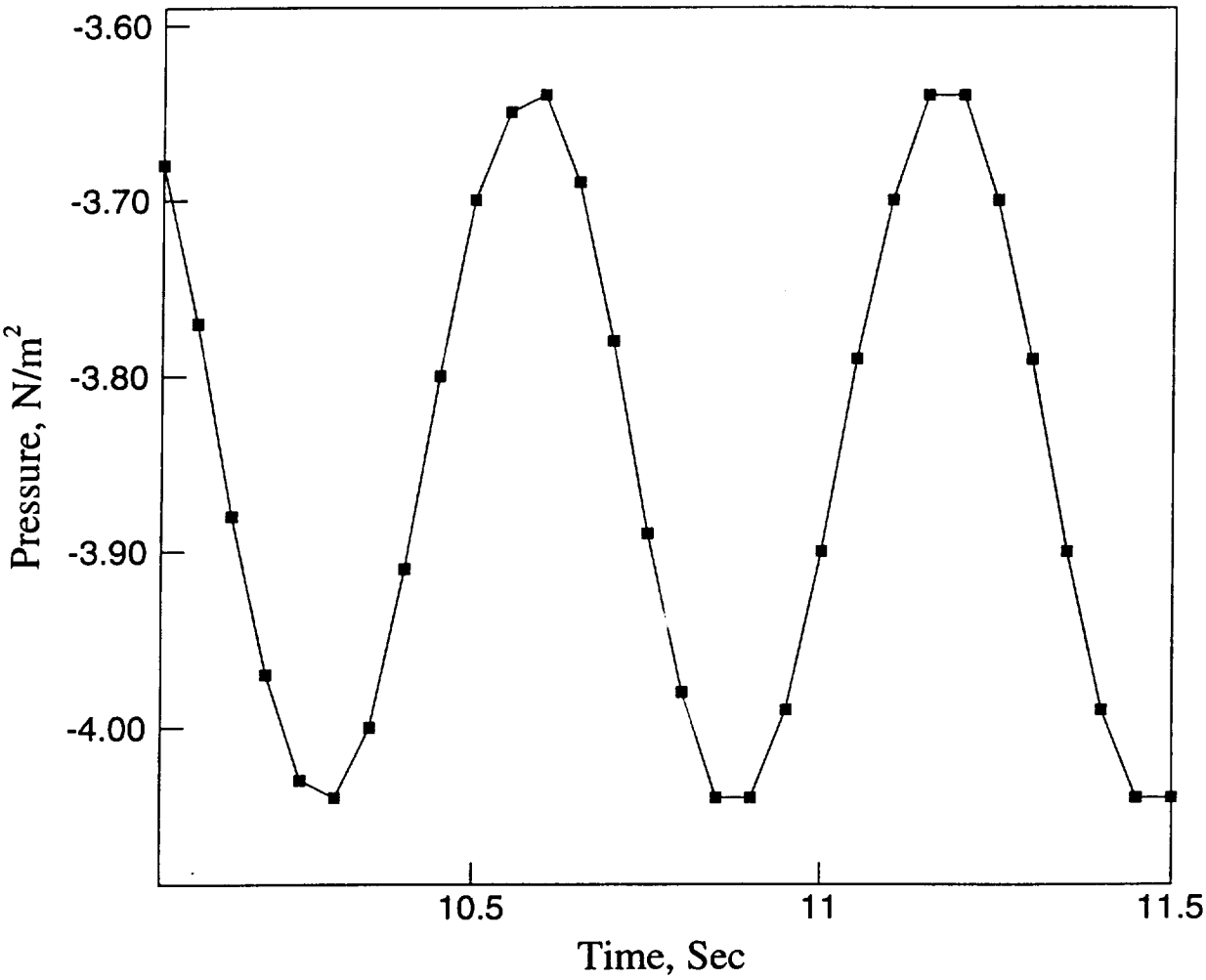

Fig. 3.2 Time history of pressure (Re = 2.5 X 10^4)

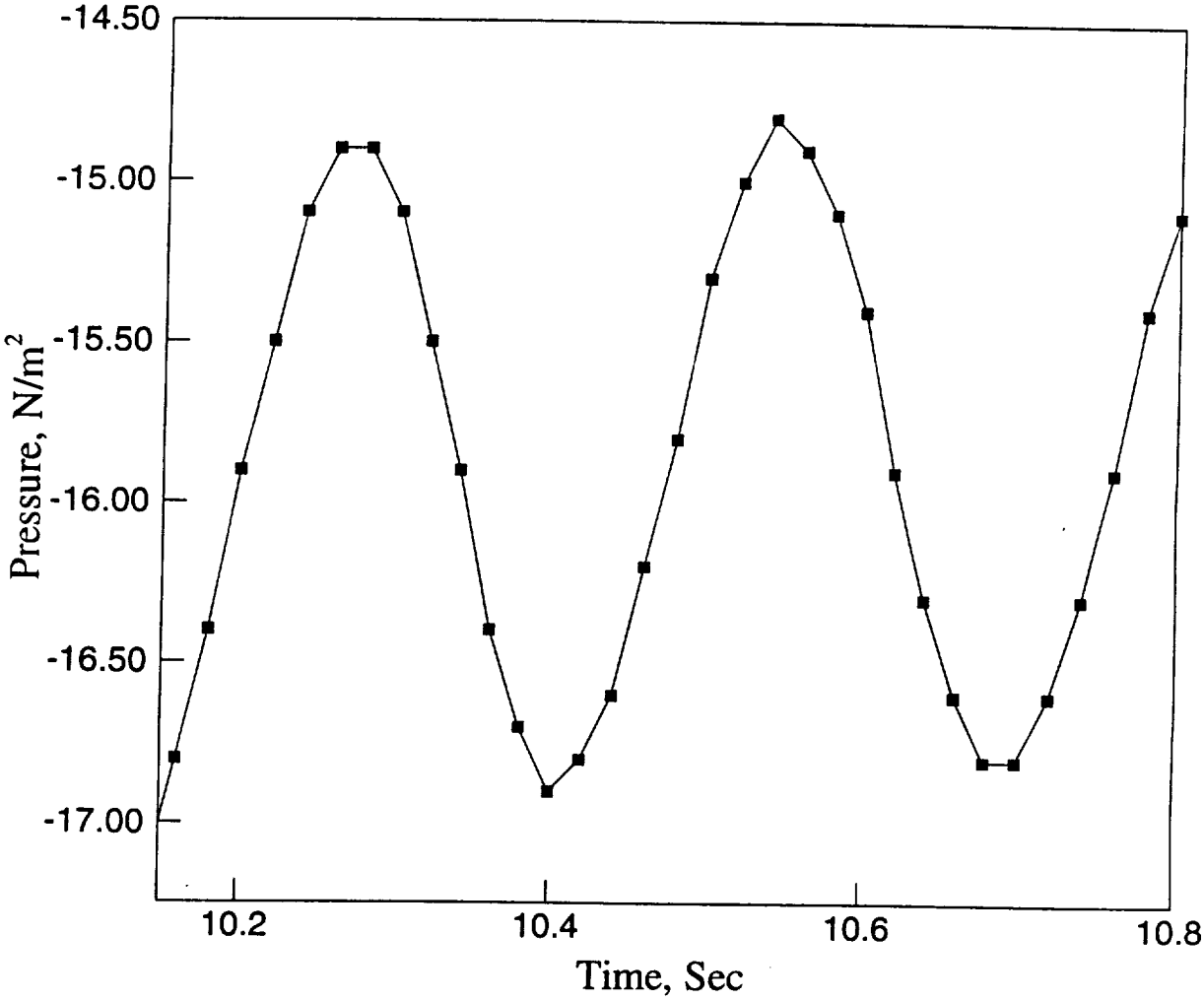

Fig. 3.3 Time history of pressure (Re = 5.0 X 10^4)

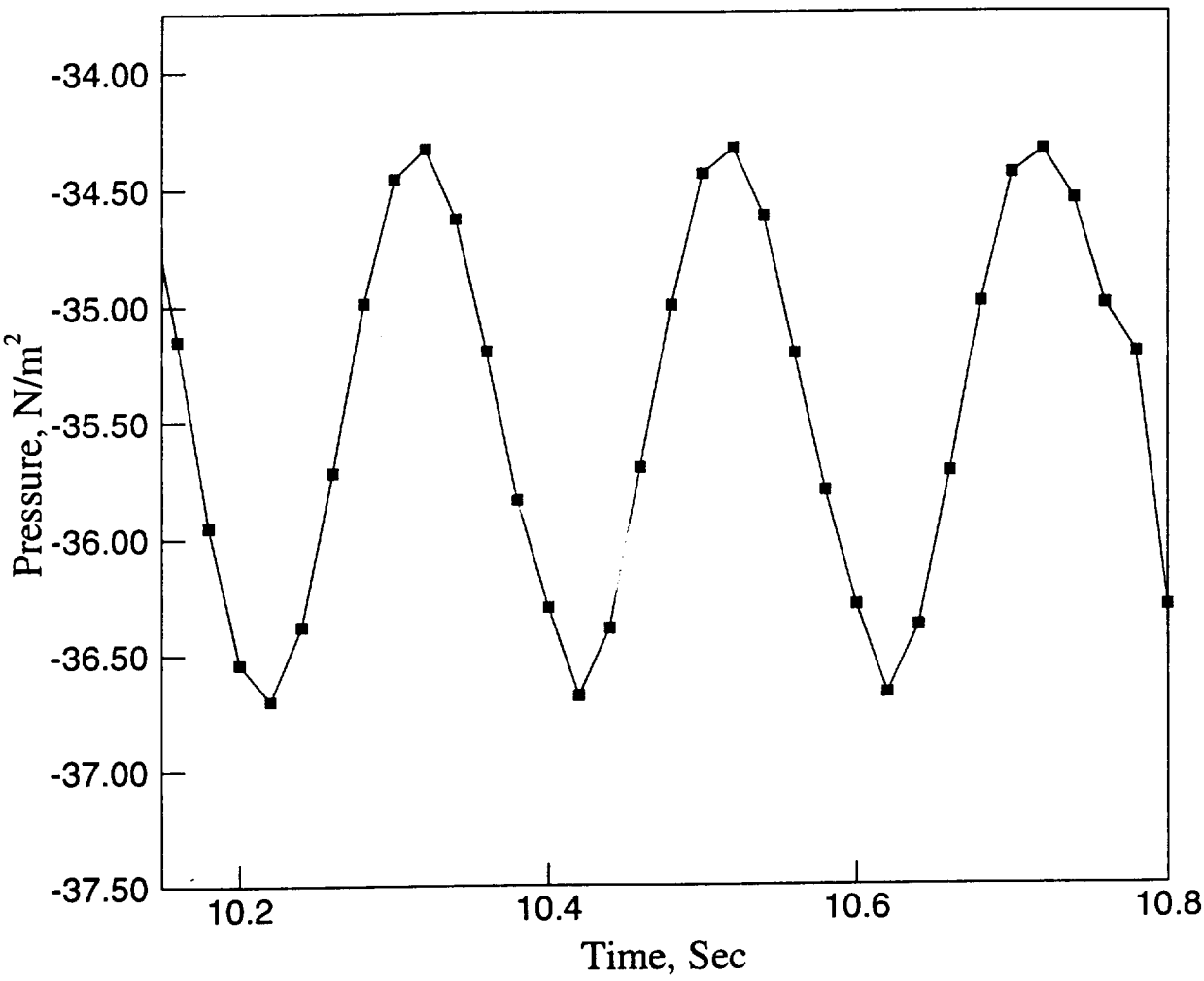

Fig. 3.4 Time history of pressure (Re = 7.5 X 10^4)

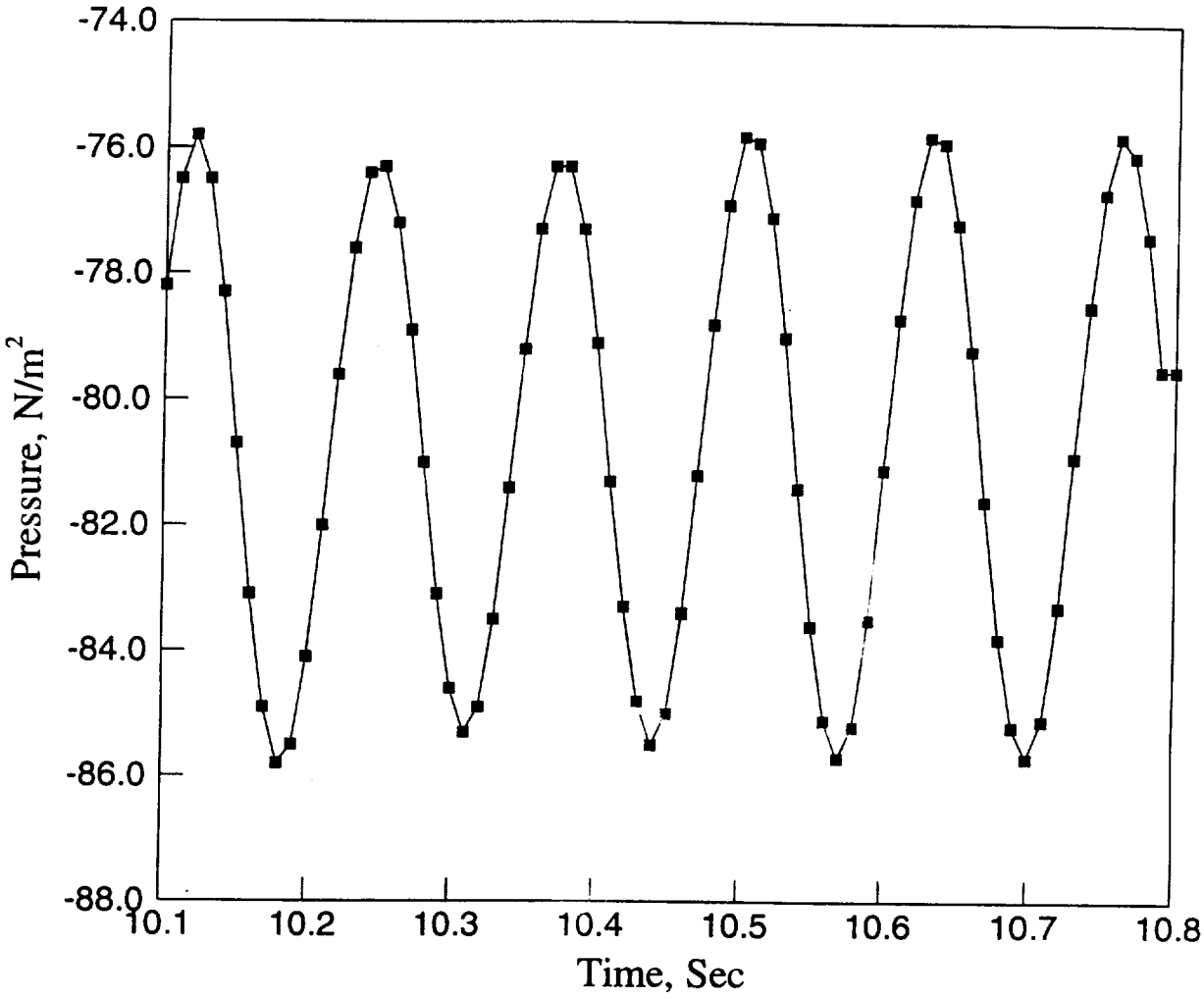

Fig. 3.5 Time history of pressure (Re = 1.25 X 10^5)

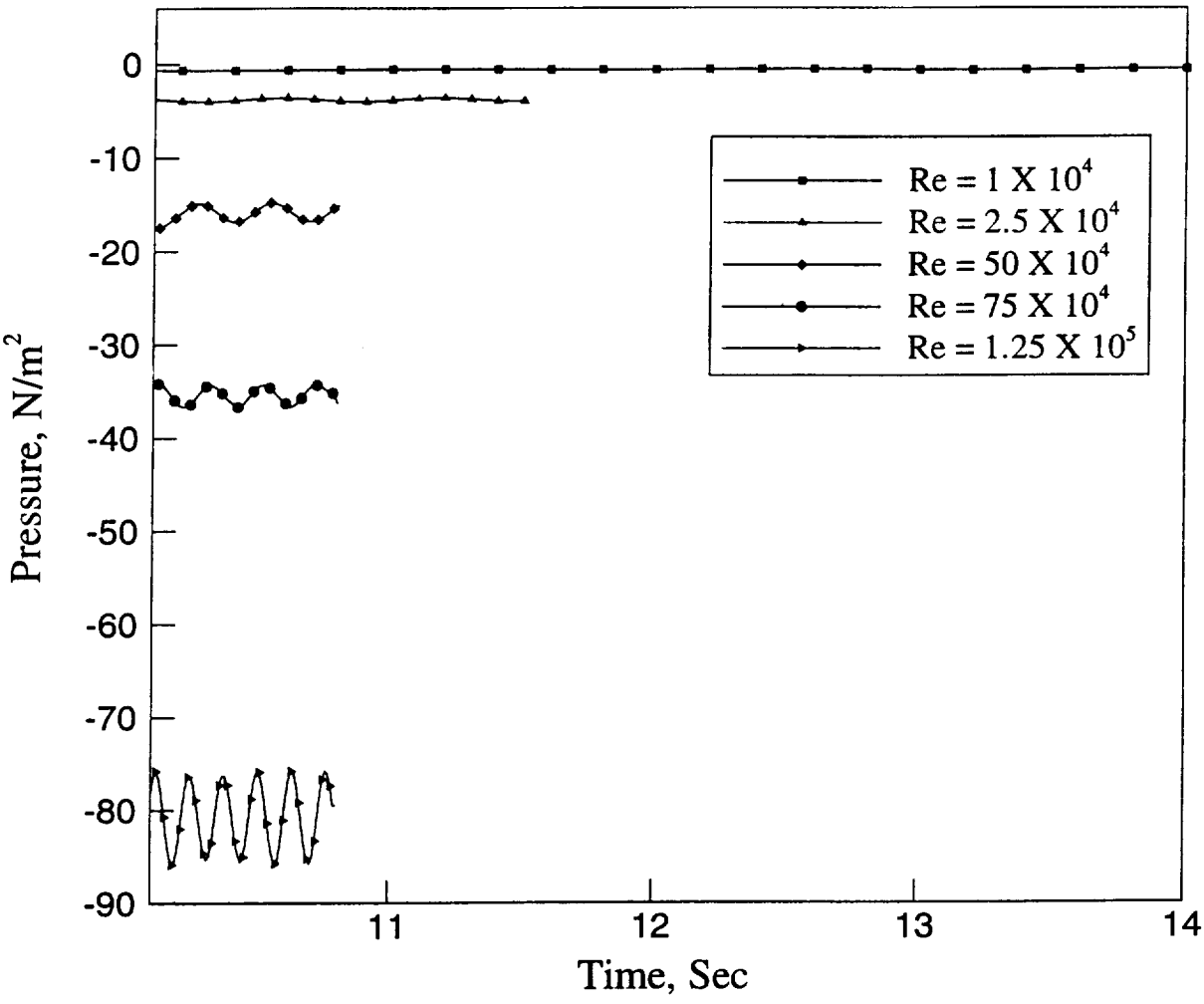

Fig. 3.6 Time history of pressure (Re = 1 X10^4 - 1.25 X10^5)

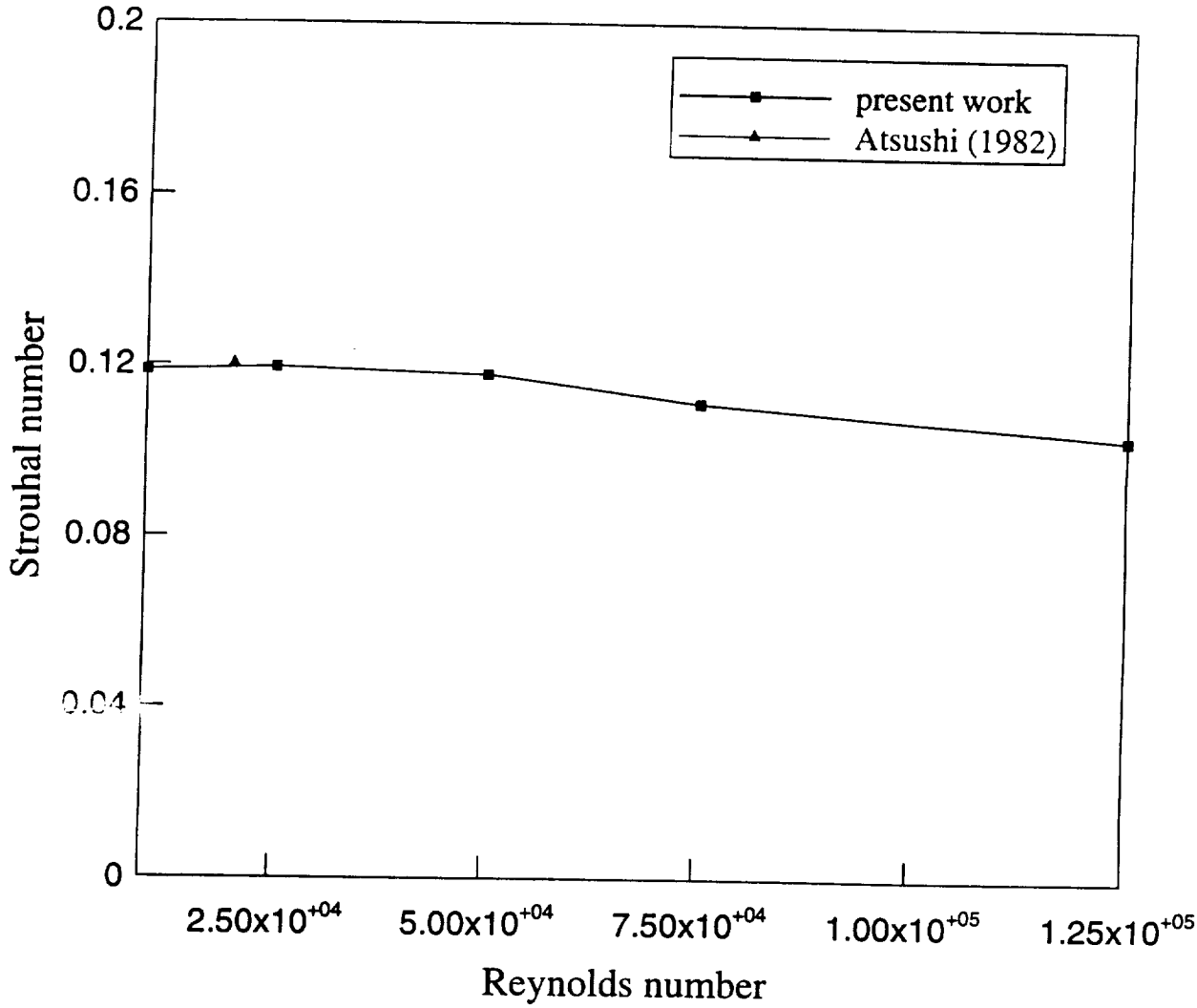

Fig. 3.7 Variation of Strouhal number with Reynolds number

[5] measured experimentally the Strouhal number in the range of the free stream Reynolds number between 70 and 2 X 10^4. In this range of Reynolds numbers, it was reported that the Strouhal number of the square cylinder showed slight and continuous change around a constant value of 0.125. The present result also compares well with the measured value of the Strouhal number by Bearman and Truman [3]. Once again, the comparison is restricted to the lower Reynolds number range due to non-availability of data at higher Reynolds number range.

The Strouhal numbers are also estimated for different aspect ratios. Figure 3.8 shows the fluctuations of pressure for aspect ratio equal to 0.8 and 1.5. Table 3.3 presents the estimated values of the Strouhal number for different aspect ratios when Reynolds number is equal to 1 X 10^4. The value of the Strohaul number nearly remained constant with the aspect ratio considered in this study.

The base pressure coefficient along the down stream face (base) is estimated next. Here, the base pressure coefficient is obtained by taking average over a number of cycles, once systematic periodic oscillation is established. The variation of the base pressure coefficient with Reynolds number is shown in Fig. 3.9. Experimental value obtained by Bearman and Truman [3] matches well with the estimated value of the base pressure coefficient. Once again, comparison is restricted to the lower Reynolds number range.

Next, drag and lift coefficients are plotted versus time for different Reynolds numbers considered in this study. These plots are shown in Figs. 3.10 - 3.19. The systematic oscillations can be seen in these plots. Average lift and drag coefficients are listed in Table 3.4 for different Reynolds numbers. Comparison of estimated average drag coefficients is also made with experimentally measured values at the lower Reynolds number range which is shown in Table 3.5. The value of drag coefficient given by Nakaguchi *et al.* is taken from the paper by Beraman and Truman [3]

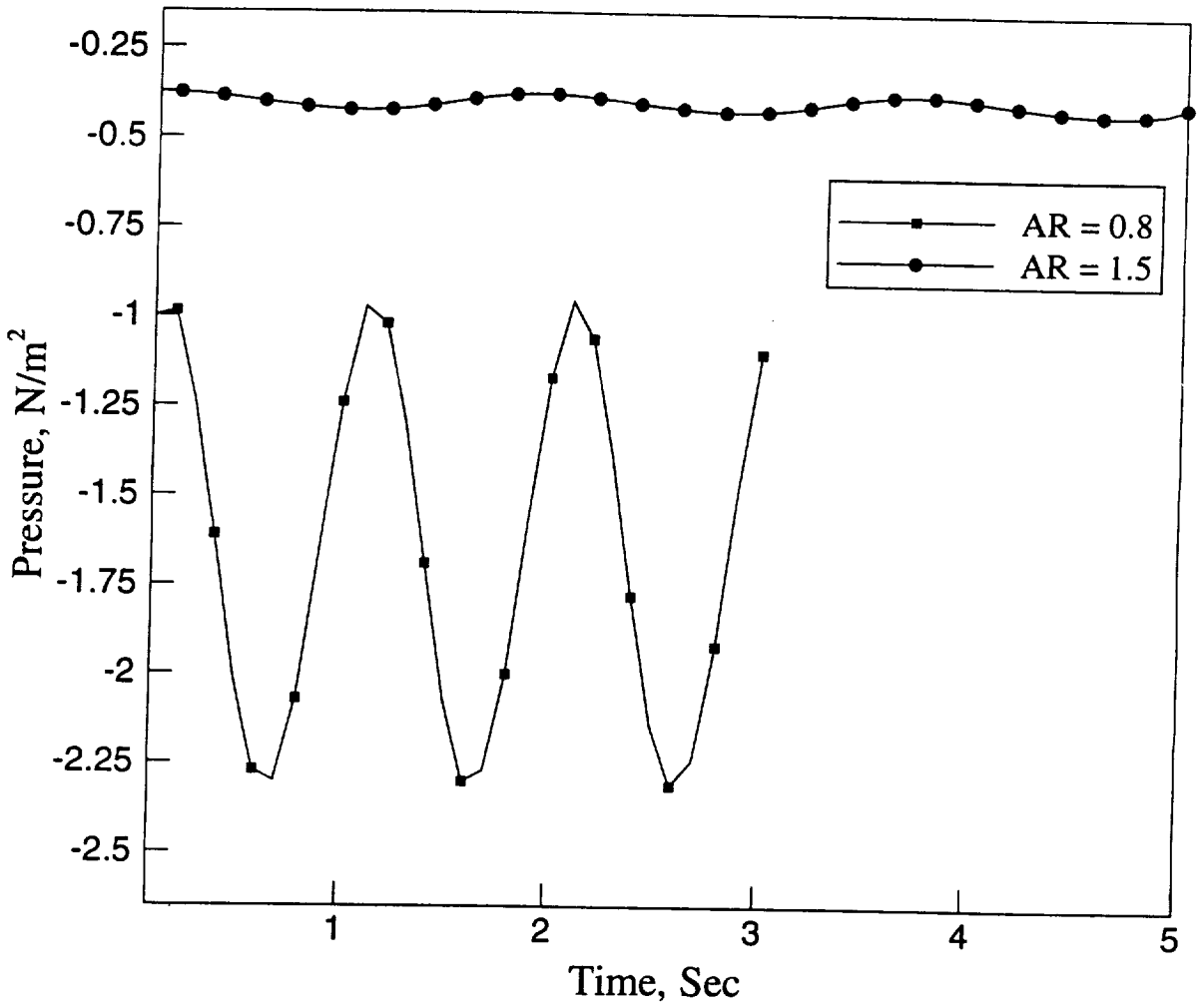

Fig. 3.8 Time history of pressure for different aspect ratios (Re = 1 X10^4)

Table 3.3. Variation of Strouhal number with aspect ratio (Re = $1X10^4$)

Aspect ratio	0.8	1.0	1.5
Strouhal number	0.1311	0.1187	0.1338

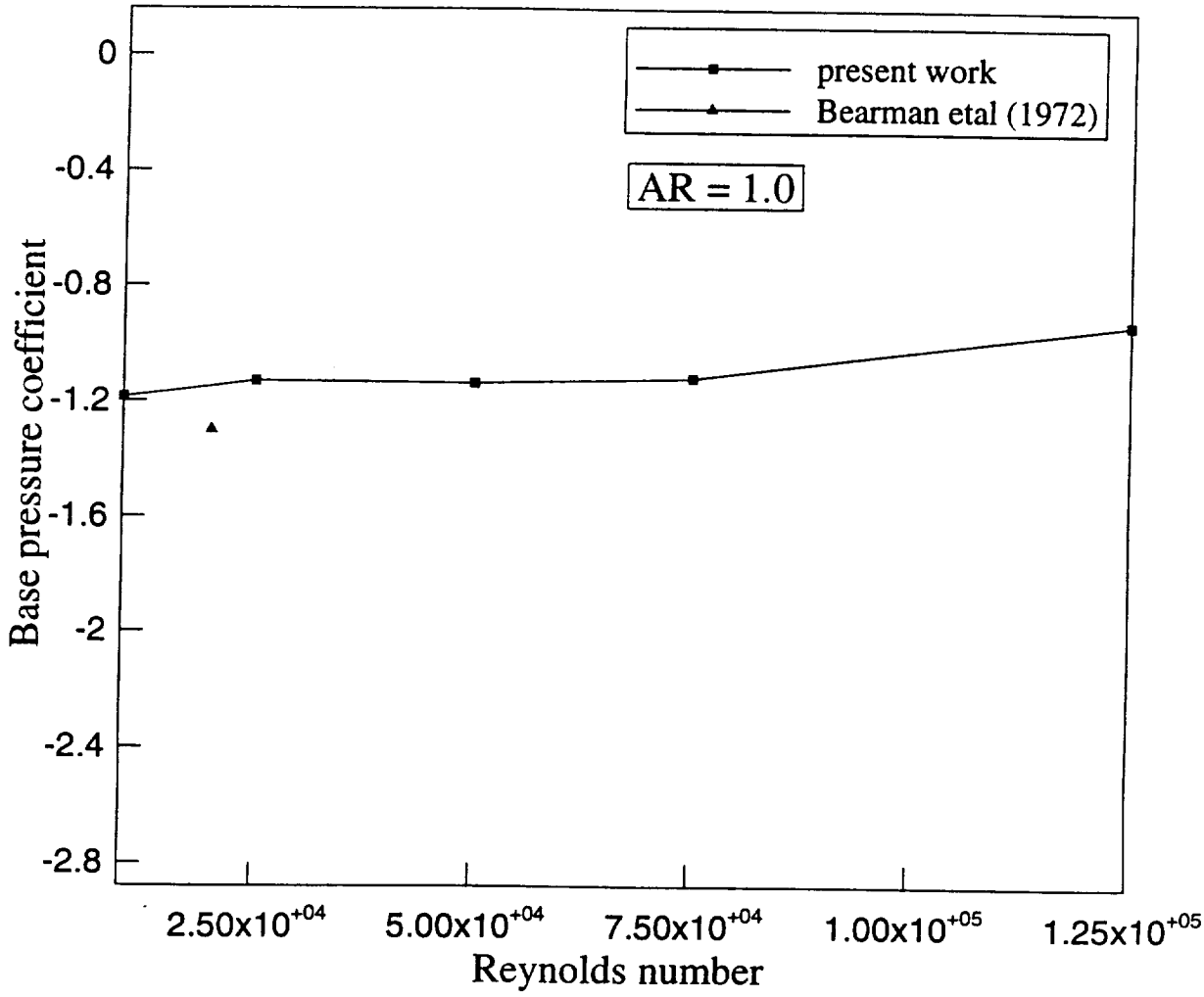

Fig. 3.9 Variation of base pressure coefficient with Reynolds number

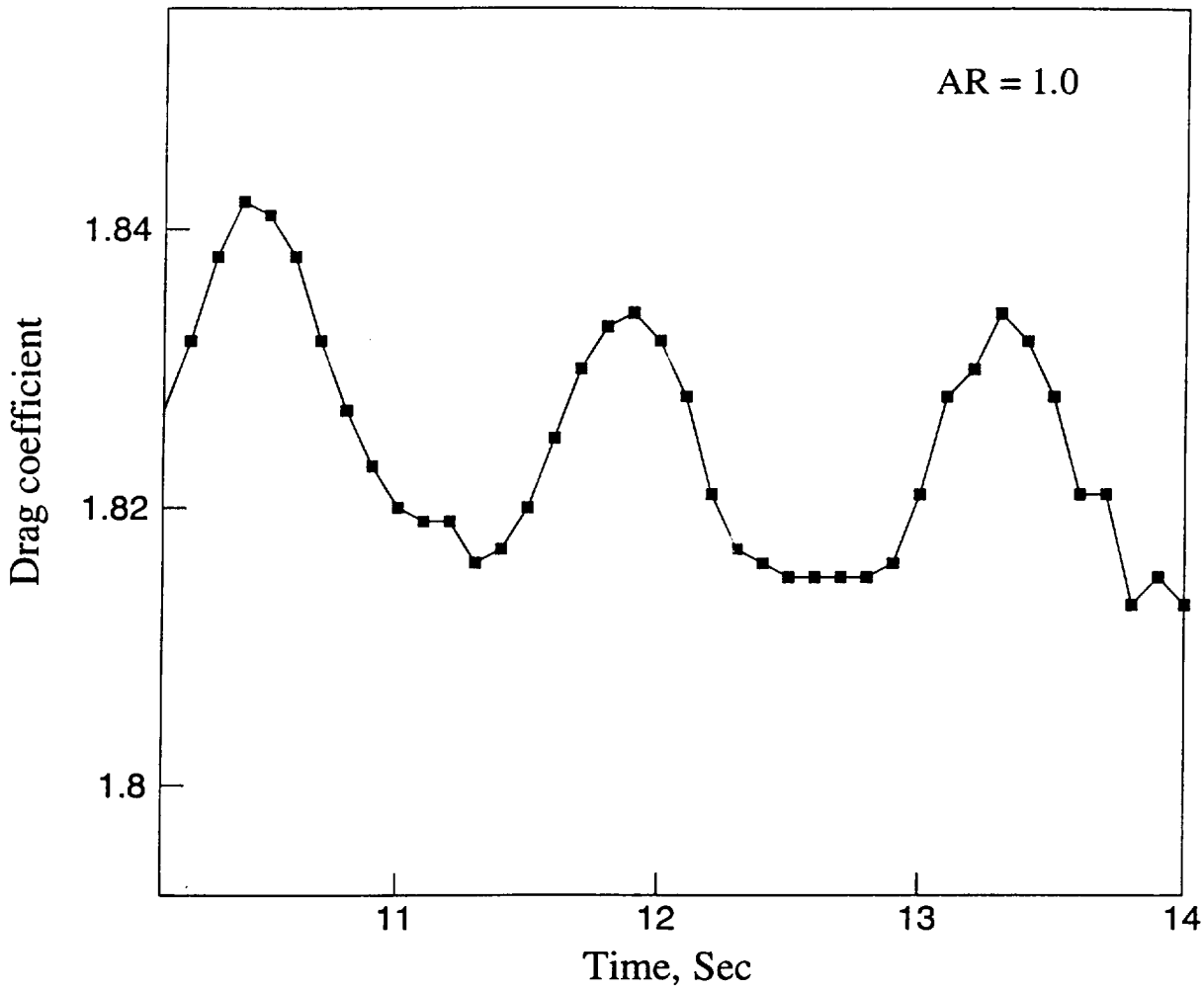

Fig. 3.10 Time history of drag coefficient (Re = 1 X 10^4)

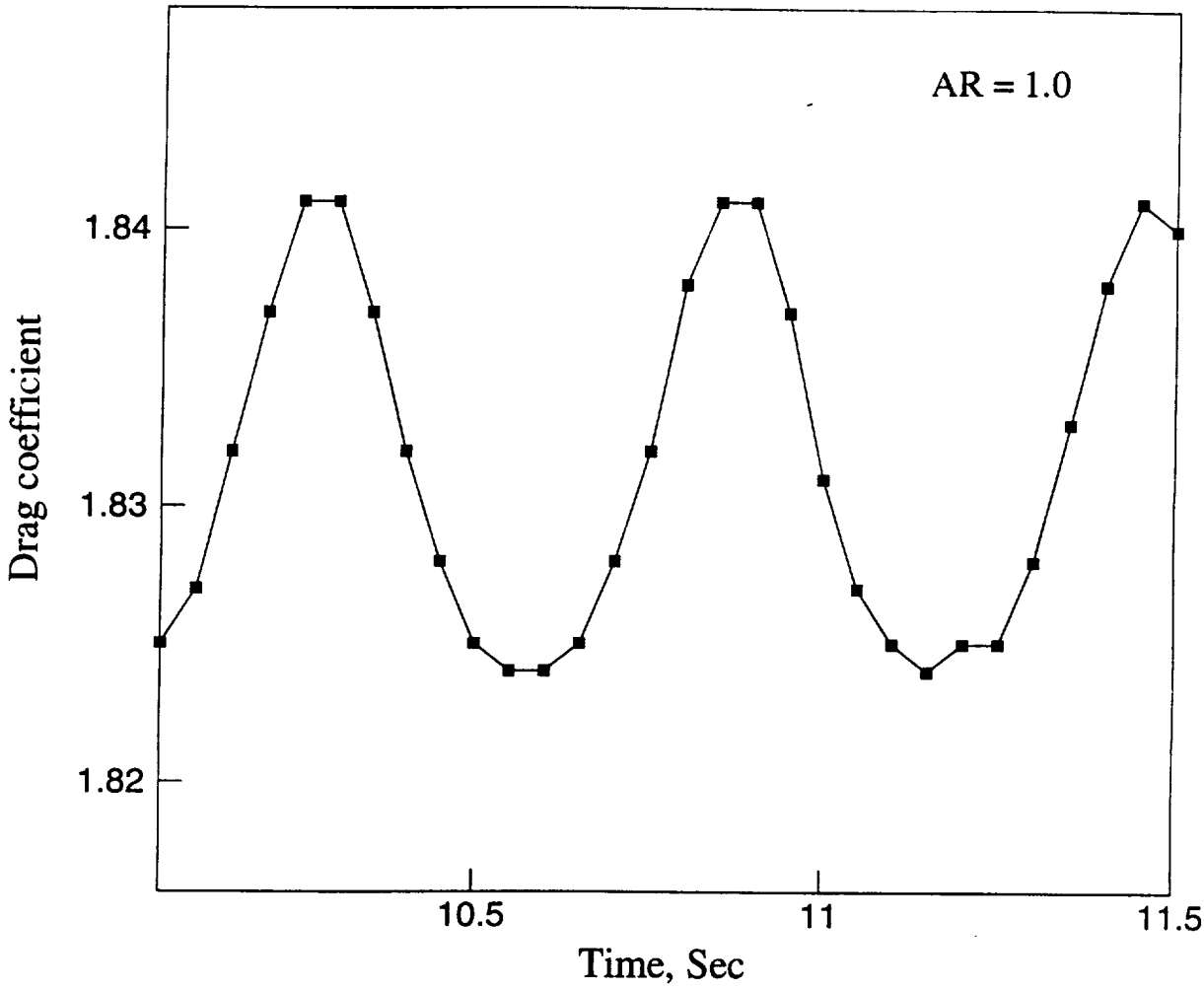

Fig. 3.11 Time history of drag coefficient (Re = 2.5 X 10^4)

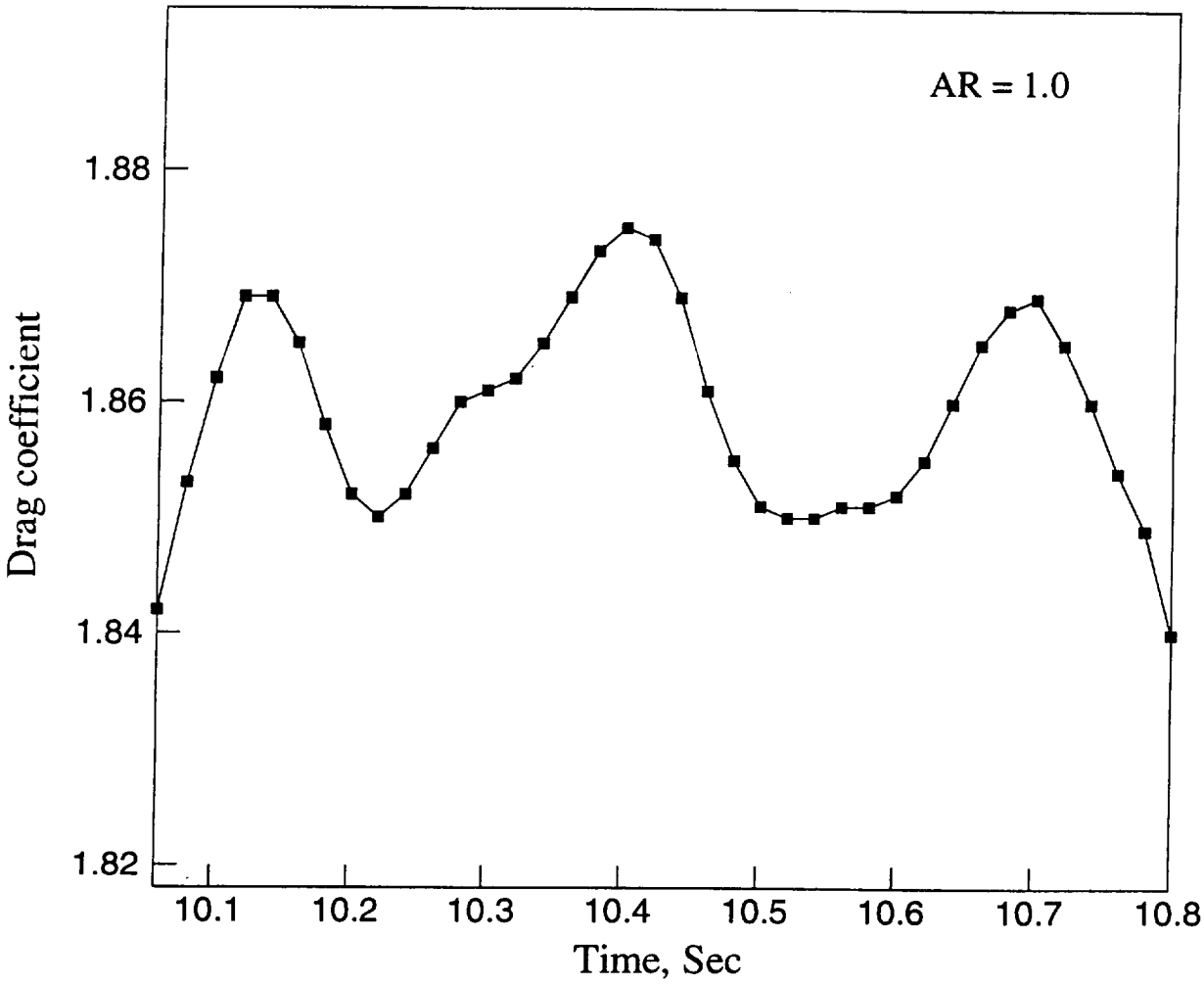

Fig. 3.12 Time history of drag coefficient (Re = 50 X 10^4)

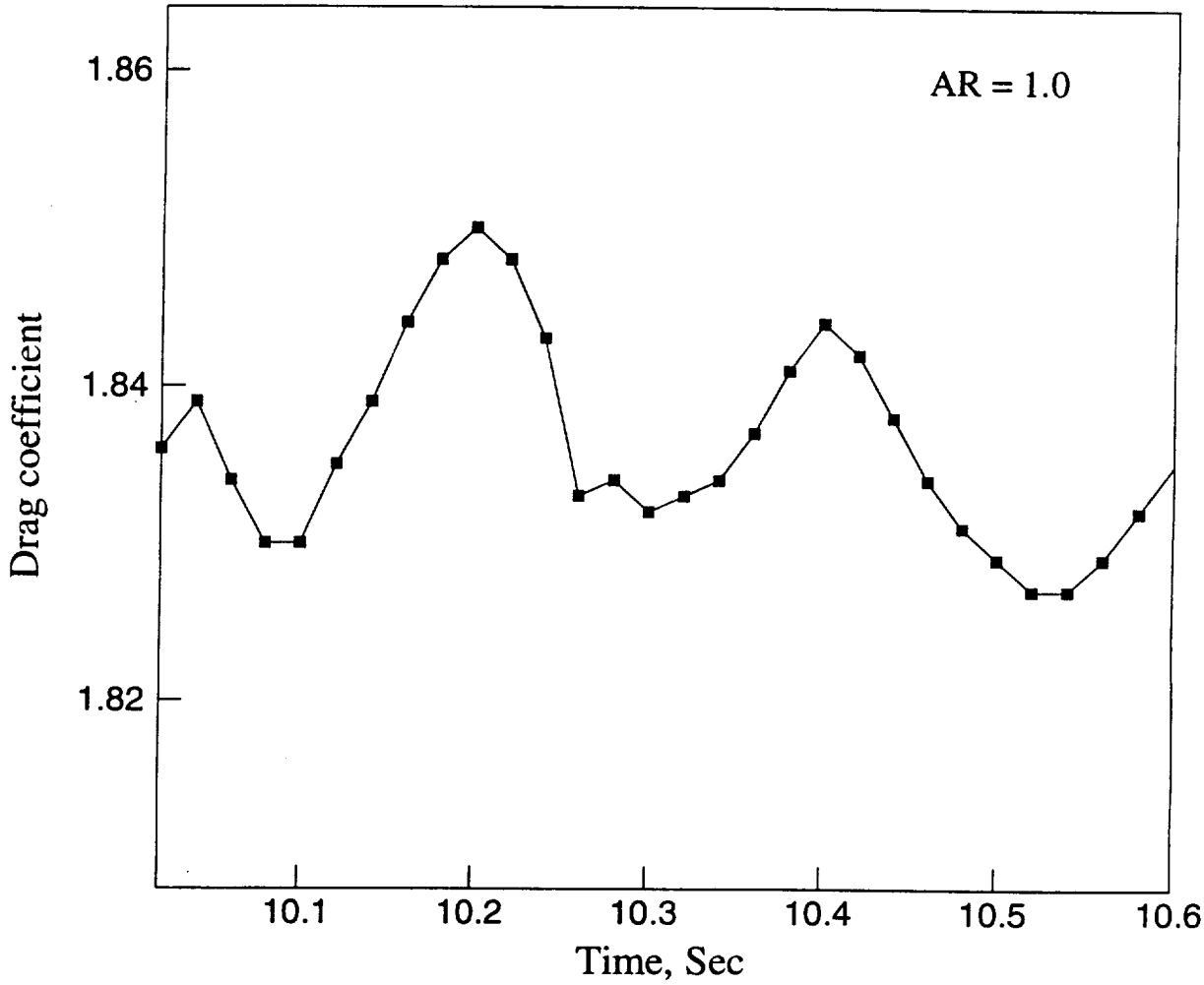

Fig. 3.13 Time history of drag coefficient (Re = 75 X 10^4)

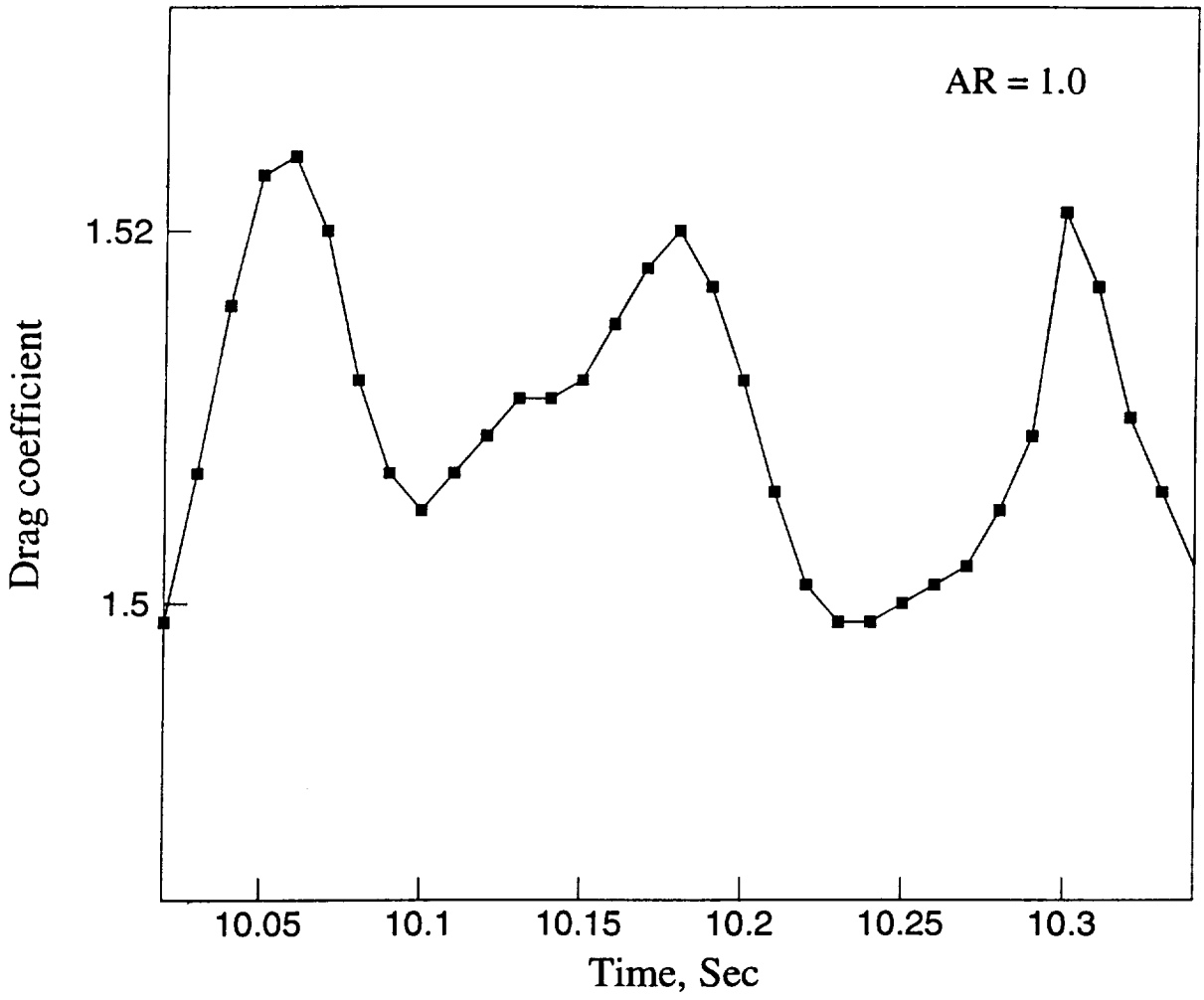

Fig. 3.14 Time history of drag coefficient (Re = 1.25 X 10^5)

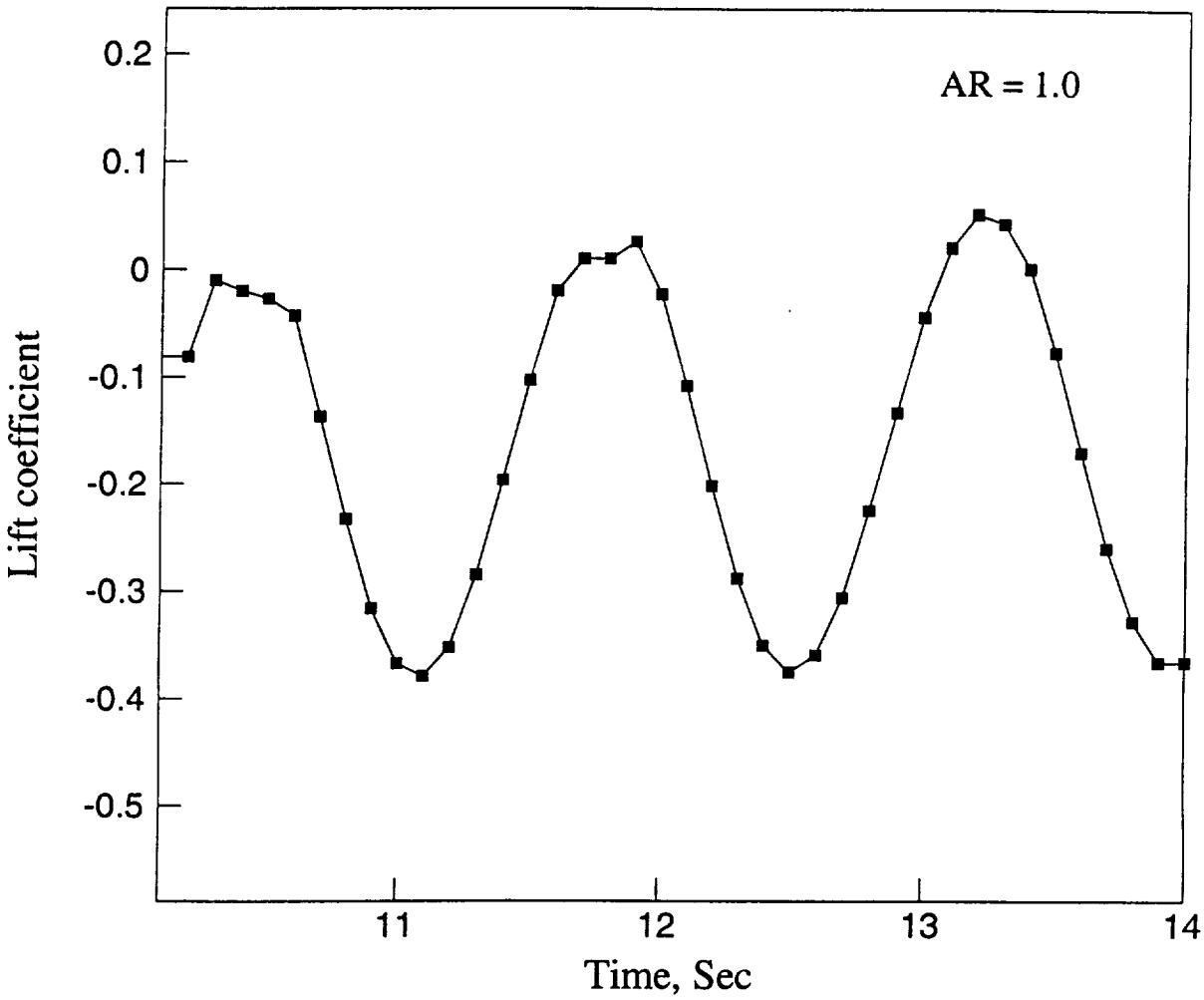

Fig. 3.15 Time history of lift coefficient (Re = 1 X 10^4)

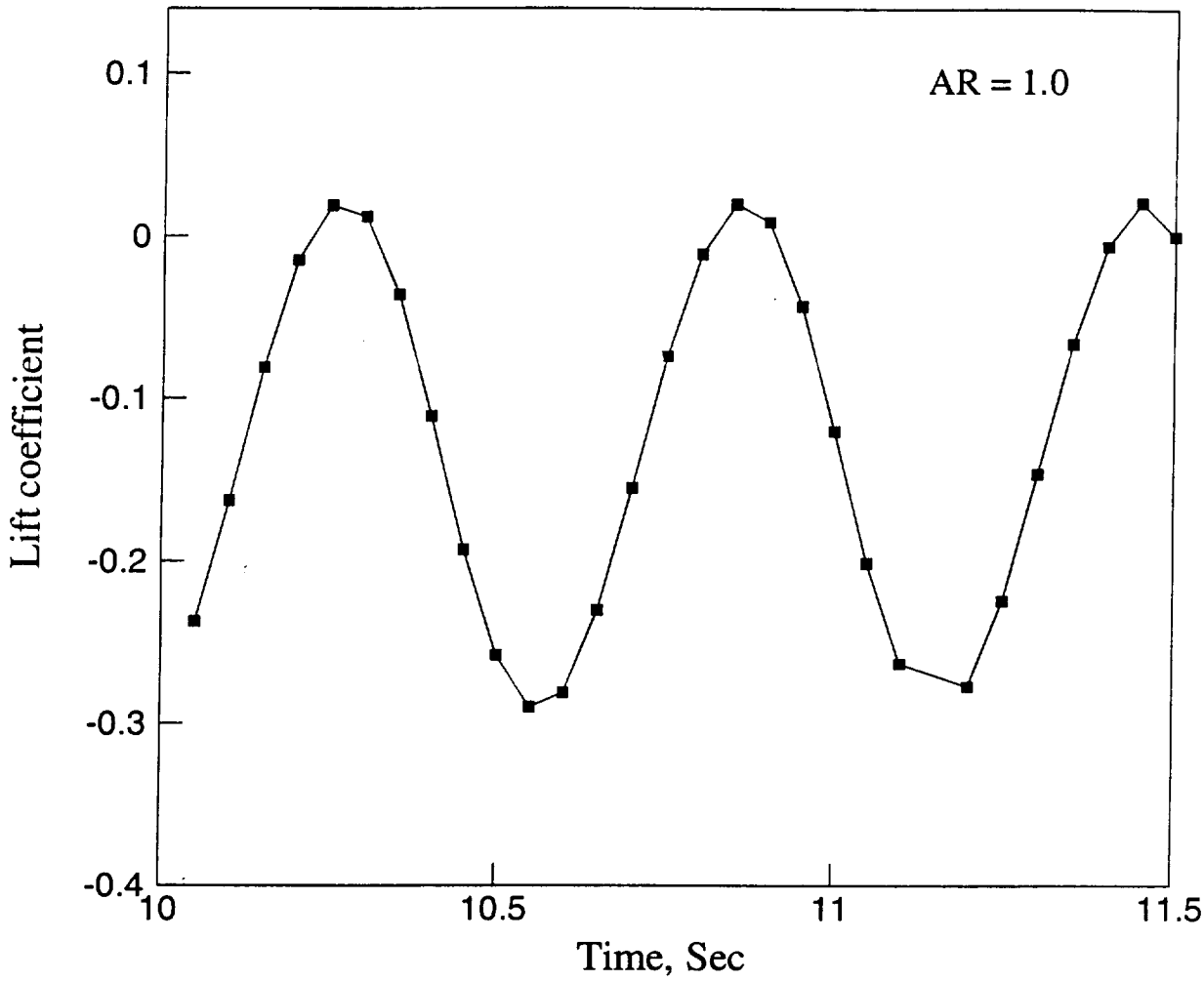

Fig. 3.16 Time history of lift coefficient (Re = 2.5 X 10^4)

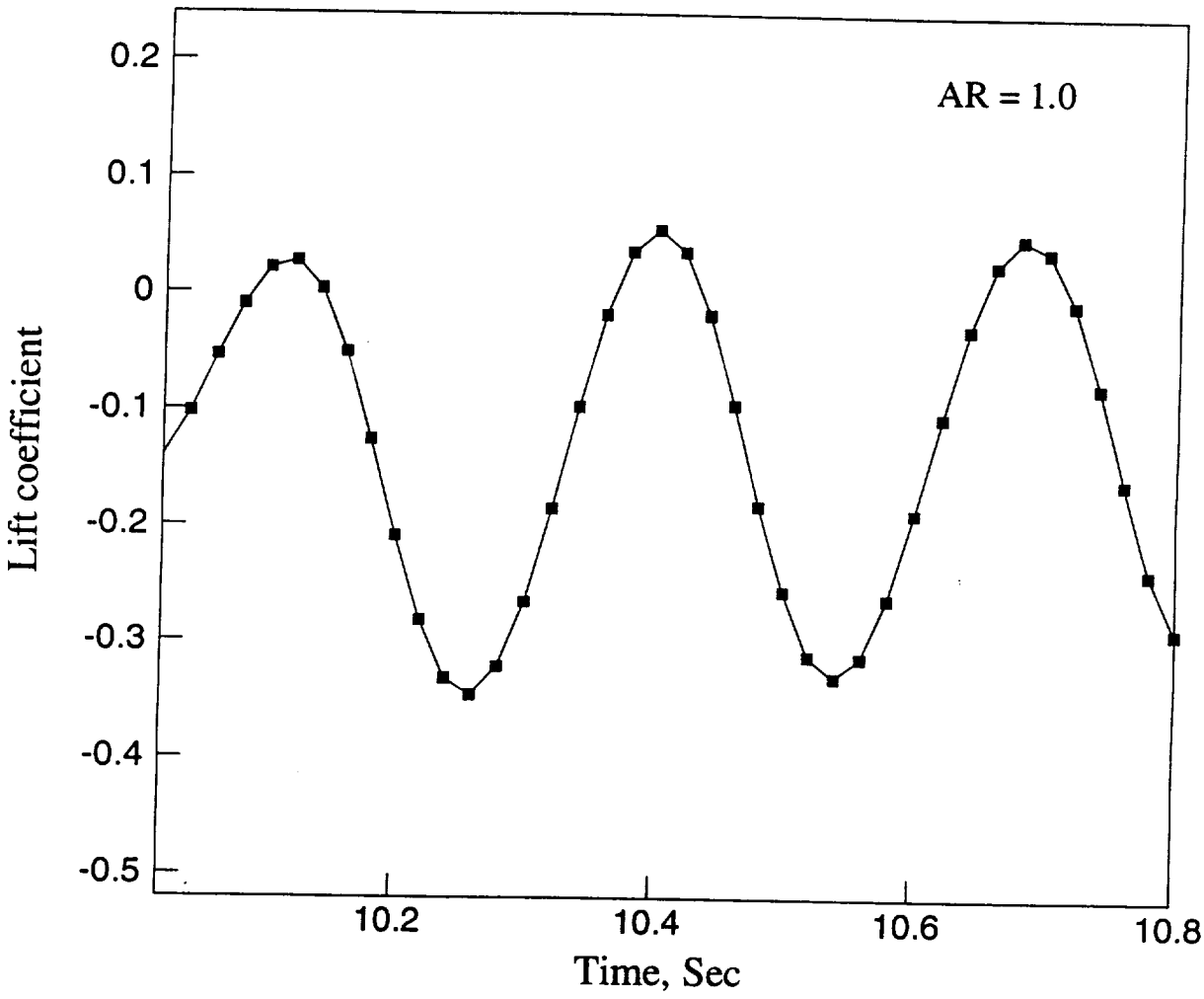

Fig. 3.17 Time history of lift coefficient (Re = 5.0 X 10^4)

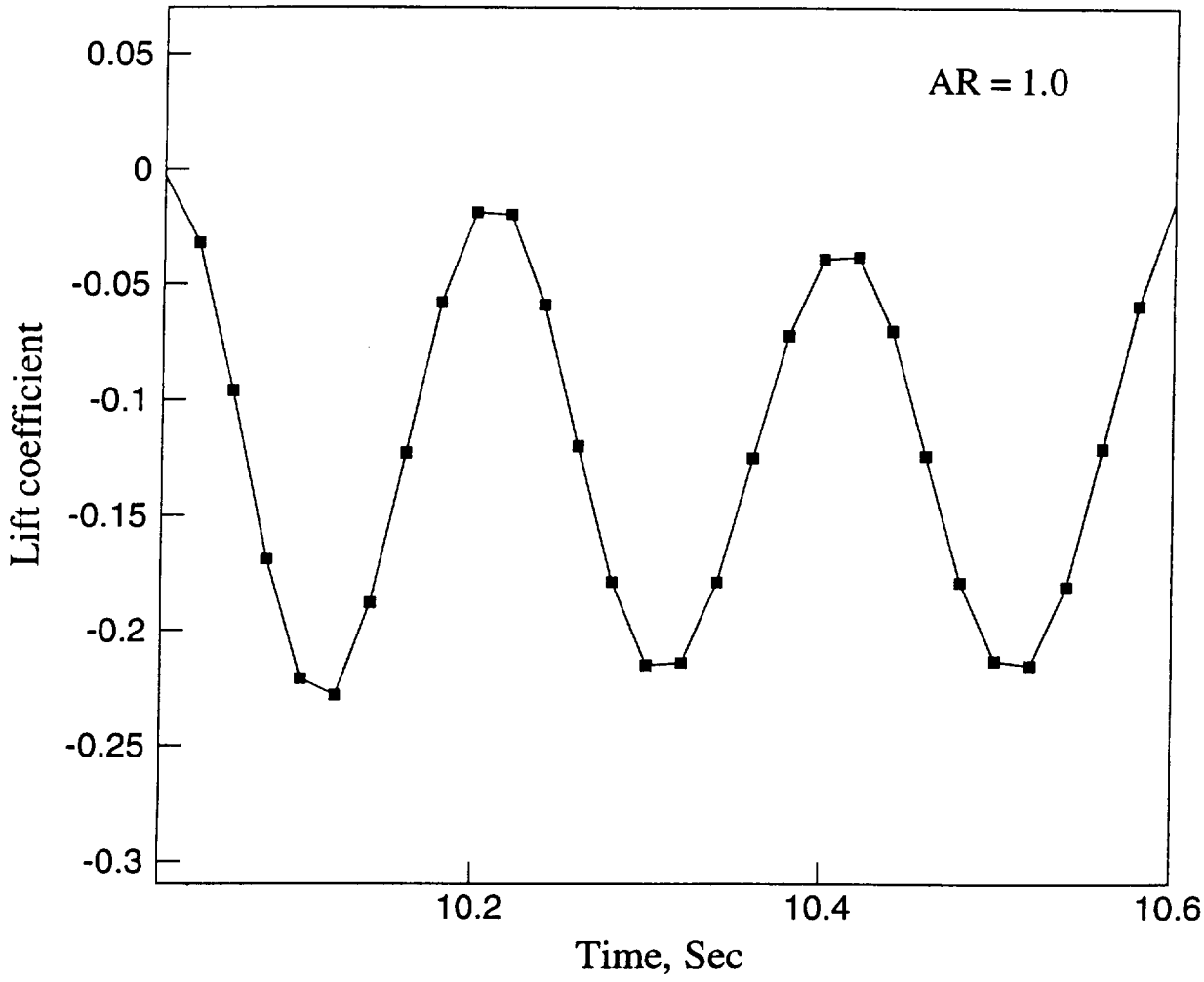

Fig. 3.18 Time history of lift coefficient (Re = 7.5 X 10^4)

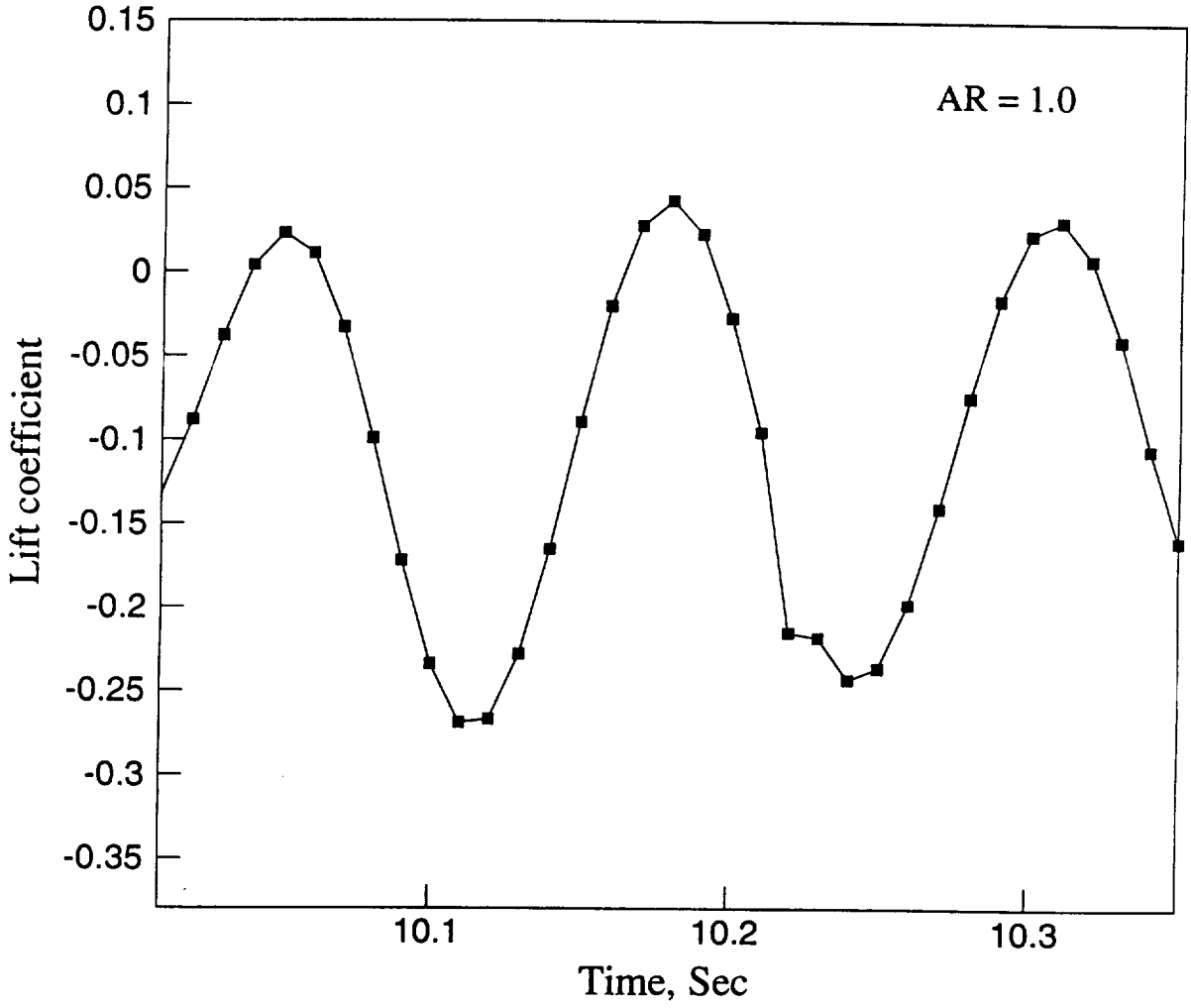

Fig. 3.19 Time history of lift coefficient (Re = 1.25 X 10^5)

Table 3.4 Variation of C_d and C_l with Re number

Reynolds number	1×10^4	2.5×10^4	50×10^4	75×10^4	1.25×10^5
Drag coefficient	1.825	1.832	1.855	1.834	1.50
Lift coefficient	0.162	0.123	0.145	0.1174	0.118

Table 3.5. Comparison of C_d with experimental value(Re = 1 X 10^4)

	Present study	Beraman and Truman [3]	Nakaguchi *et al.*
Drag coefficient	1.825	2.00	1.90

Finally, streamlines are plotted at the maximum, middle, and minimum lift coefficient points after periodic oscillation is established. Figure 3.20 shows the streamline pattern for Reynolds number of 1 X 10^4. Flow separates immediately at the leading edge, even for the lowest Reynolds number considered in this study. Similar results are presented in Figs. 3.21-3.23 for other Reynolds numbers. As can be seen from these plots, the streamline pattern changes with time. The streamline pattern also changes with increase in Reynolds number.

3.2 Case 2 : With Jet

The important reason for a jet in the rear stagnation region is for reducing the drag. A recent experimental and numerical study by Atsuchi *et al.* [10] gives information on various aspect of fluid dynamics, in the case of a circular cylinder. The cross flow over a two-dimensional circular cylinder at Re = 1X 10^5 was used as a "bench mark" test. Since, no information is available in case of rectangular cylinders, it is reasonable to make some judgements based on this work as the overall aspects of fluid dynamics is very much similar. Only effect of free stream Reynolds number is investigated. Blockage ratio, aspect ratio as well as jet blowing momentum coefficient C_m are unchanged in this study.

In case of circular cylinders, when the jet blowing momentum coefficient is lower than 0.0005, no change is seen in the drag coefficient. Drag decreases for C_m between 0.001 and 0.02 [10]. It was also noted that further increase in C_m can actually increase the drag coefficient. Although, it is not possible to draw the same conclusion with complete confidence, in case of rectangular cylinders, it was decided to use intuitively a value of 0.01 for C_m. As pointed in this section, this value of C_m helped in drag reduction. The study is conducted using the free stream Reynolds number ranging from 1 X 10^4 to 1.25 X 10^5. Also in this case (with jet), steady state

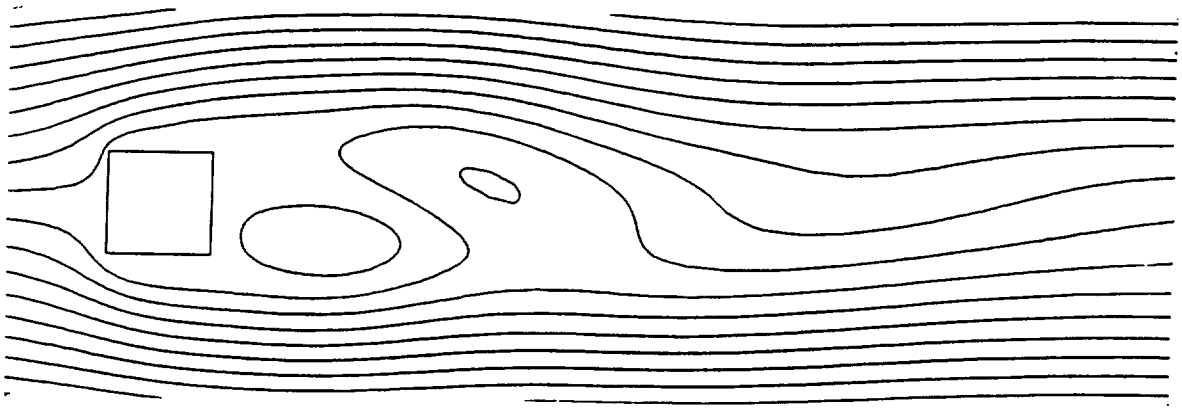

(a) At the maximum C_l point

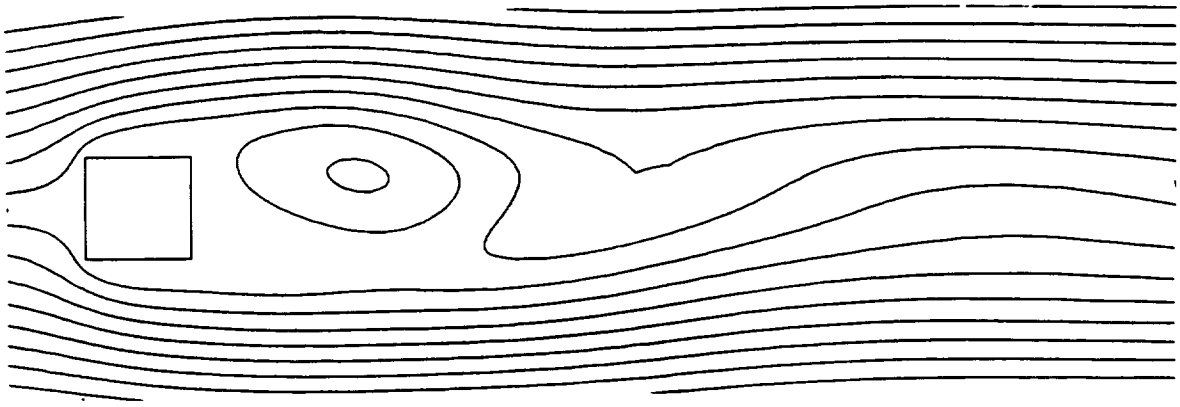

(b) At the middle C_l point

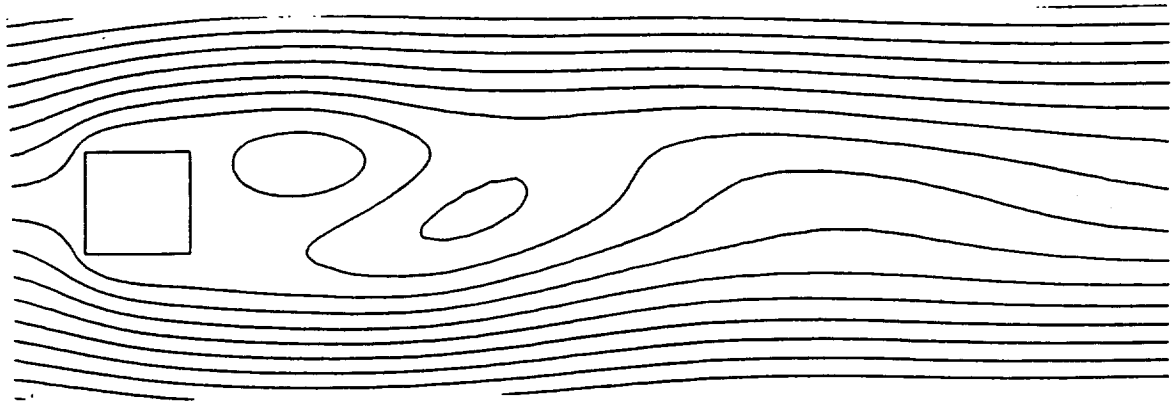

(c) At the minimum C_l point

Fig. 3.20 Streamlines from unsteady computation at Re = 1 X 10^4

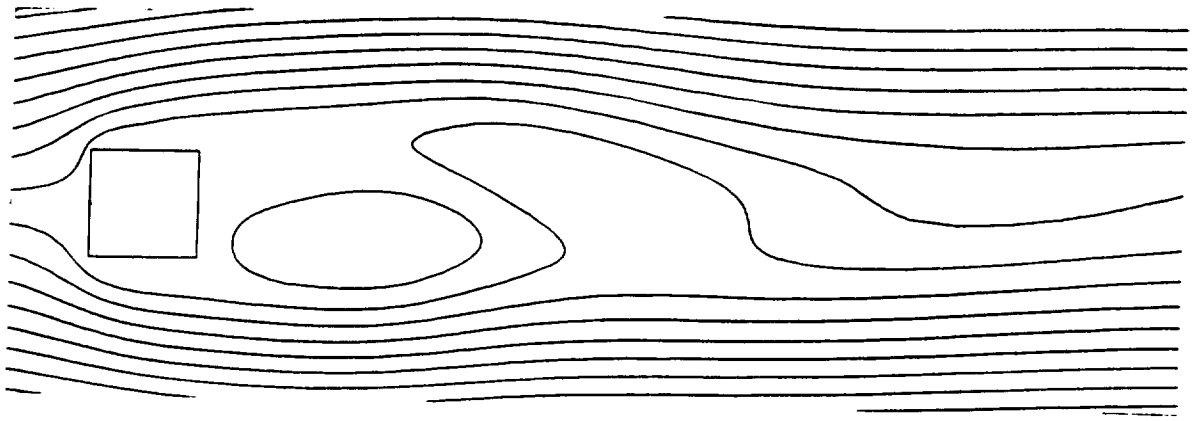

(a) At the maximum C_l point

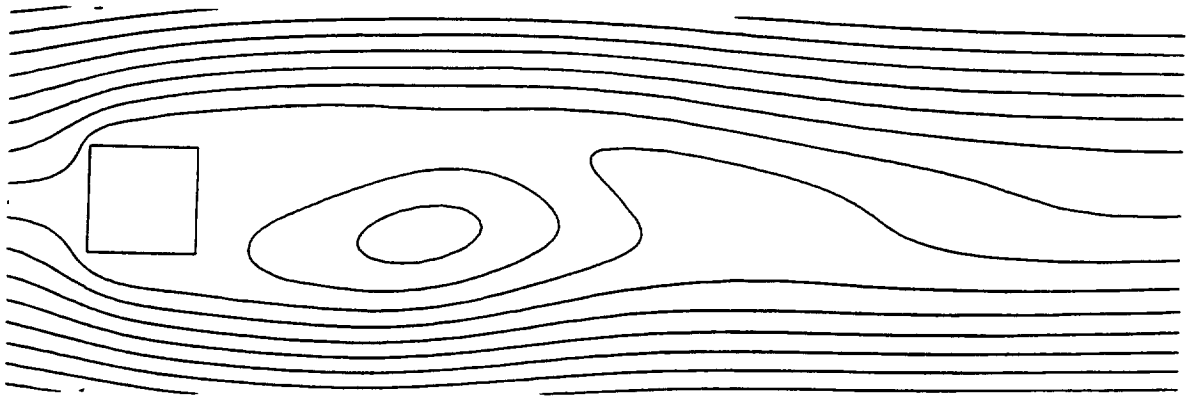

(b) At the middle C_l point

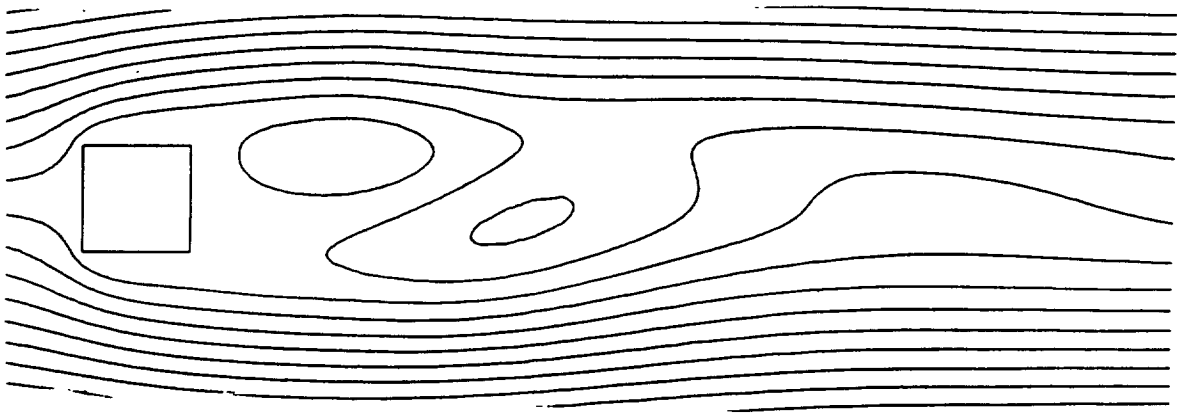

(c) At the minimum C_l point

Fig. 3.21 Streamlines from unsteady computation at Re = 2.5 X 10^4

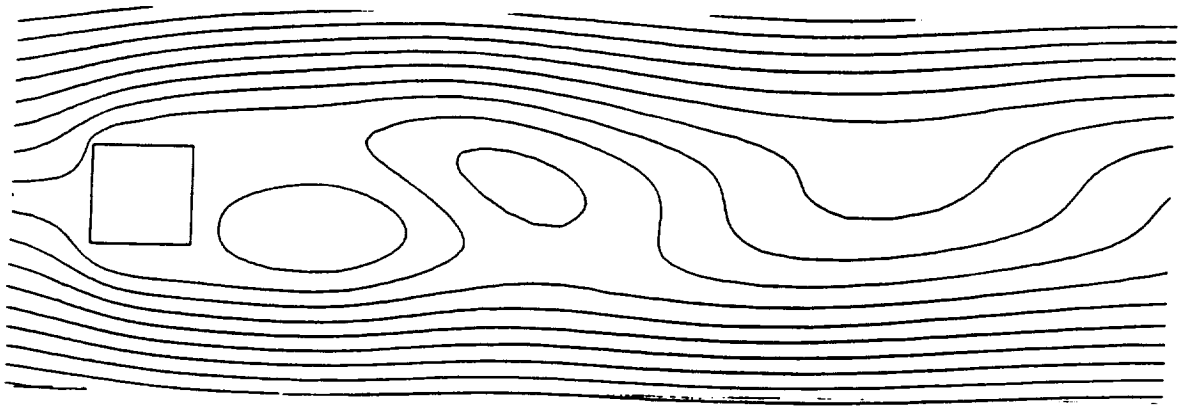

(a) At the maximum C_l point

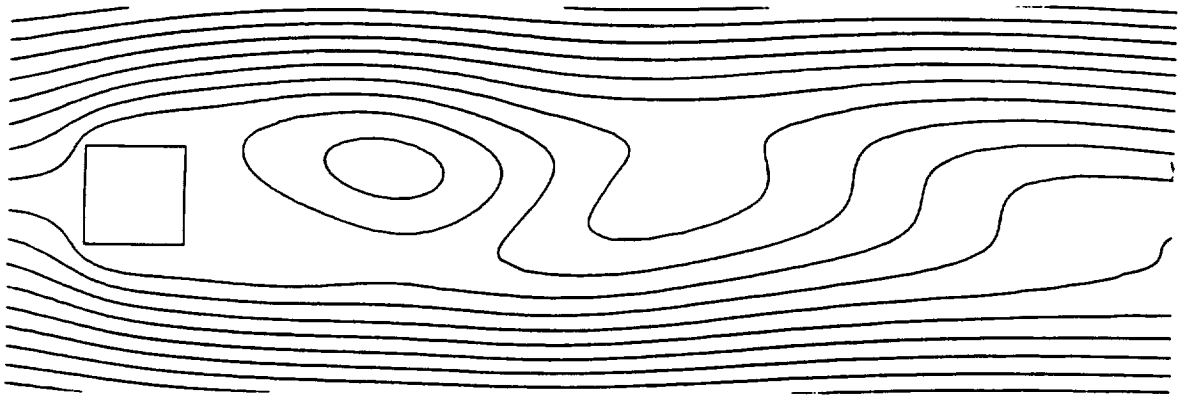

(b) At the middle C_l point

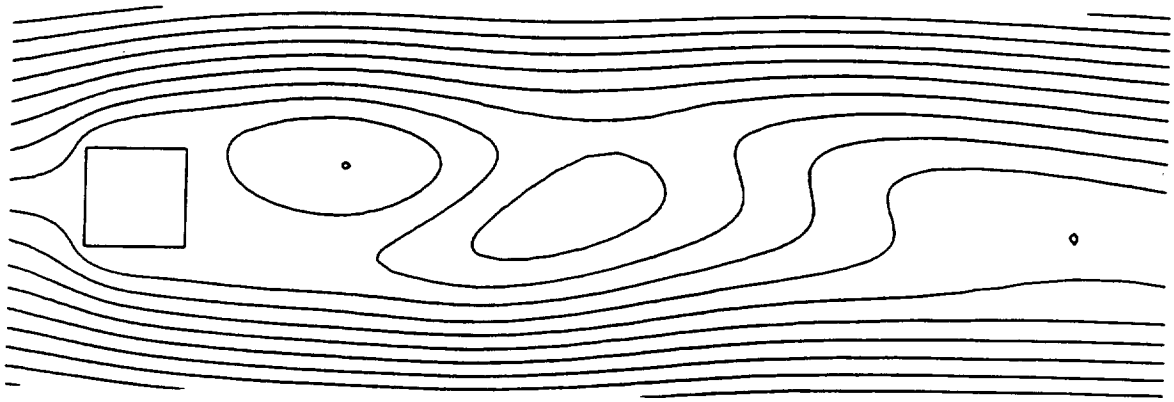

(c) At the minimum C_l point

Fig. 3.22 Streamlines from unsteady computation at Re = 5.0 X 10^4

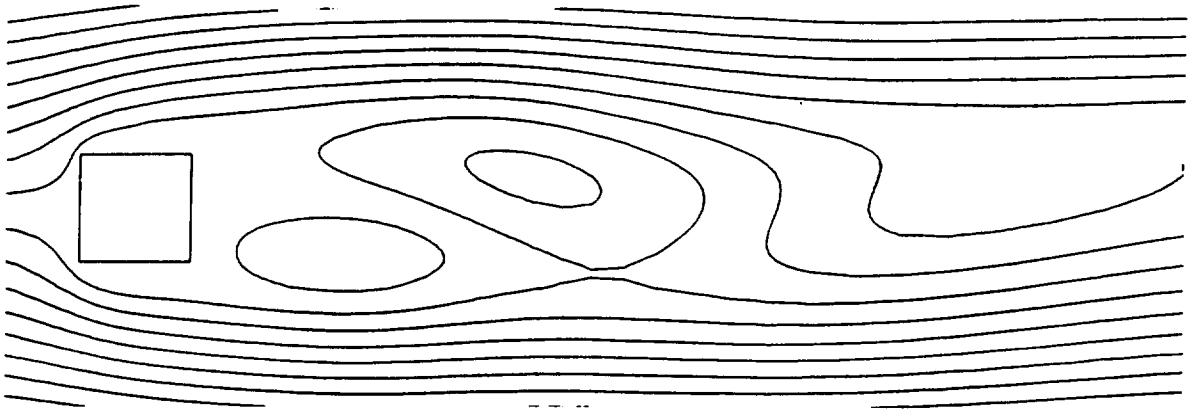

(a) At the maximum C_l point

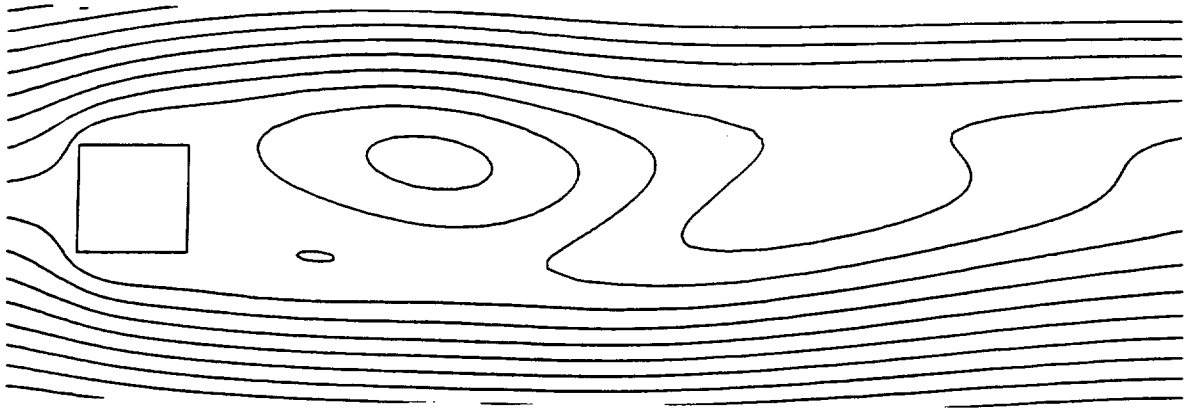

(b) At the middle C_l point

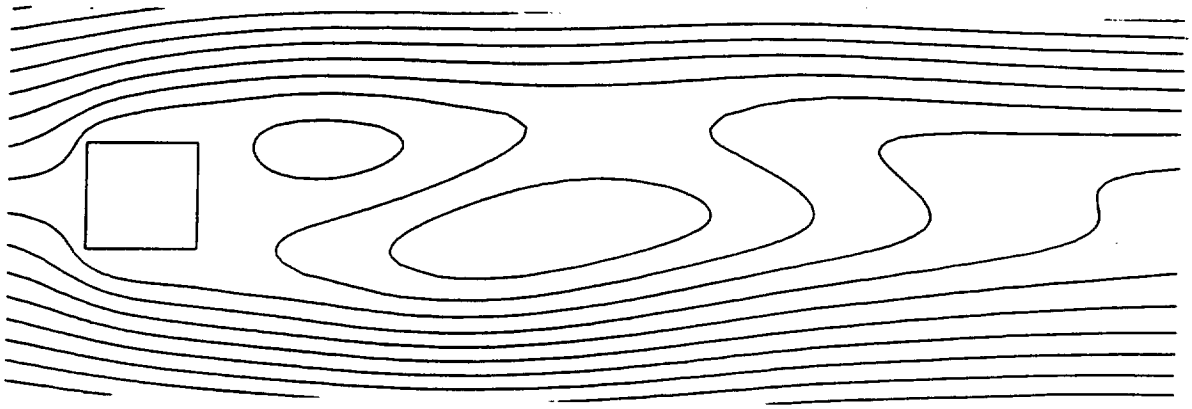

(c) At the minimum C_l point

Fig. 3.23 Streamlines from unsteady computation at Re = 7.5 X 10^4

assumption is made. Drag coefficients are listed in the Table 3.6 for different Reynolds numbers for both cases, i.e, with jets as well as without jets. It is clearly seen that the drag is reduced when jet is introduced at rear stagnation region. Only in the case of Re = 1.25 X 10^5, the change in drag is negligible.

Figure 3.24 shows streamlines plots for different free stream Reynolds numbers with C_m = 0.01. The streamline pattern becomes more symmetric when jet is introduced in the rear stagnation region which could be the reason for reduction in drag coefficient.

Further, numerical experimentation is carried out to investigate the effect of increasing C_m on drag coefficient. Drag coefficients are listed in the Table 3.7 for different values of Cm when Re = 1.25 X 10^5. The value of drag coefficient is not affected when C_m =0.0005. It decreases when the value of C_m is increased to 0.01, but further increase in C_m actually increases drag coefficient. Figure 3.25 shows streamlines plots for the different values of C_m at Re = 1.25 X 10^5. The position and size of recirculation zone clearly changes with the value of C_m which is the main reason for affecting the drag coefficient.

Table 3.6 Value of C_d with jet and no jet for different free stream Re number

Reynolds number	1×10^4	25×10^4	50×10^4	75×10^4	1.25×5
Drag coefficient (without jet)	1.825	1.832	1.855	1.834	1.50
Drag coefficient (with jet, C_m =0.01)	1.557	1.596	1.60	1.534	1.55

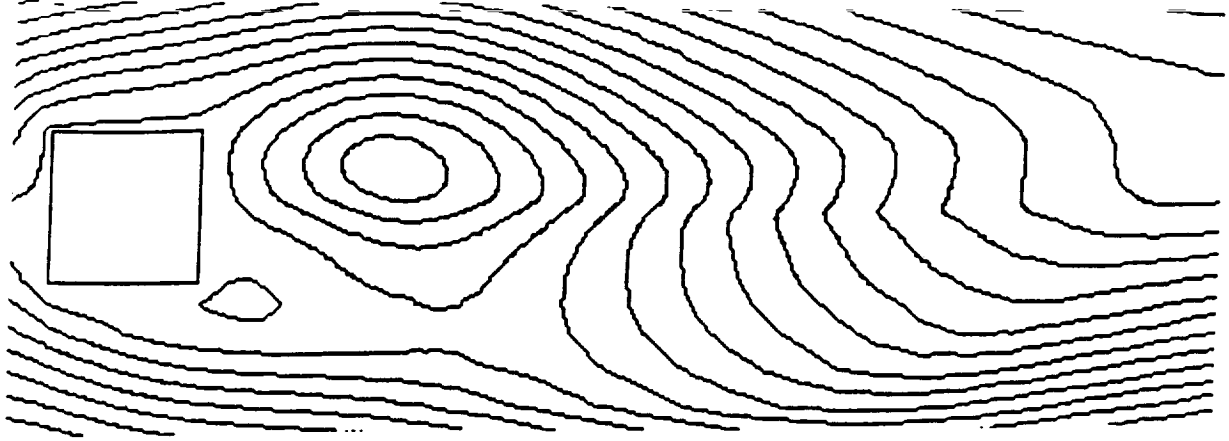

(a) At Re = 1 X 10^4

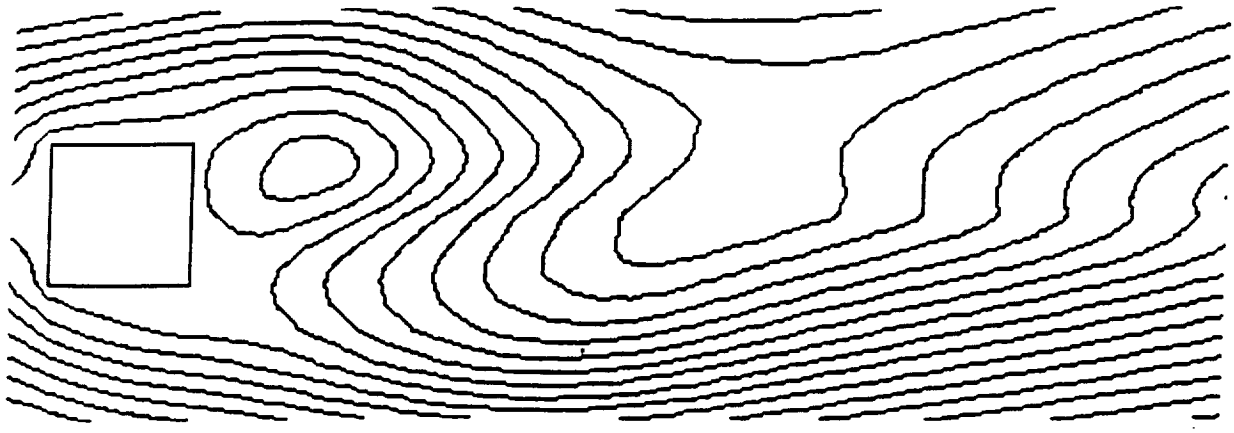

(b) At Re = 5 X 10^4

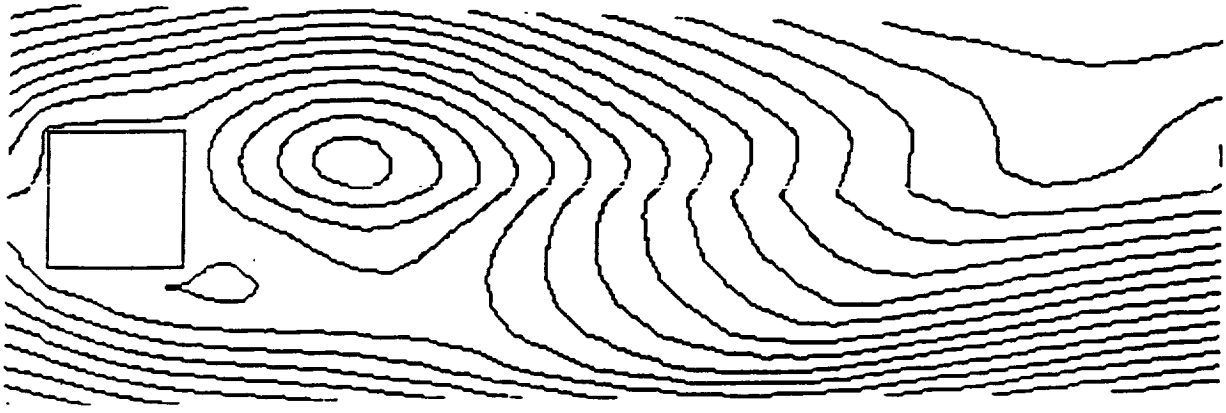

(c) At Re = 1.25 X 10^5

Fig. 3.24 Streamlines from steady computation ($C_m = 0.01$)

Table 3.7 Value of C_d for different C_m at Re = 1.25 X 10^5

C_m	0.0005	0.01	0.02	0.05
Drag coefficient, C_d	1.83	1.55	1.89	1.90

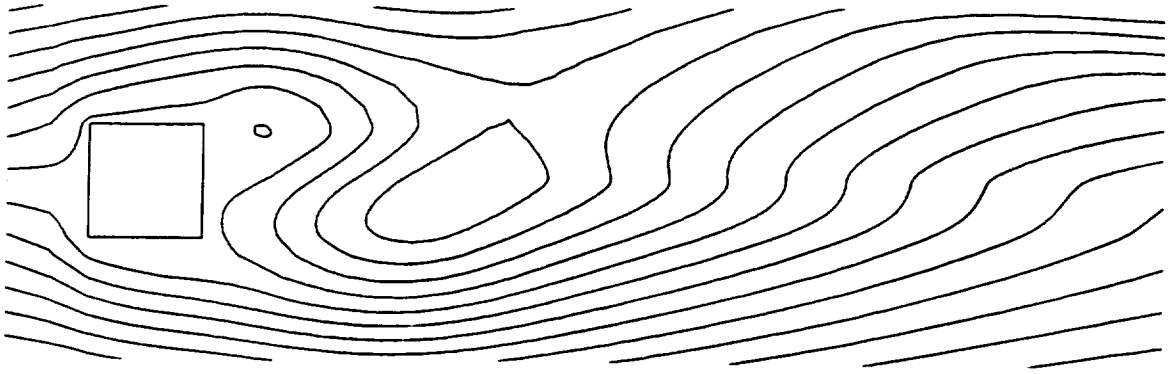

(a) $C_m = 0.0005$

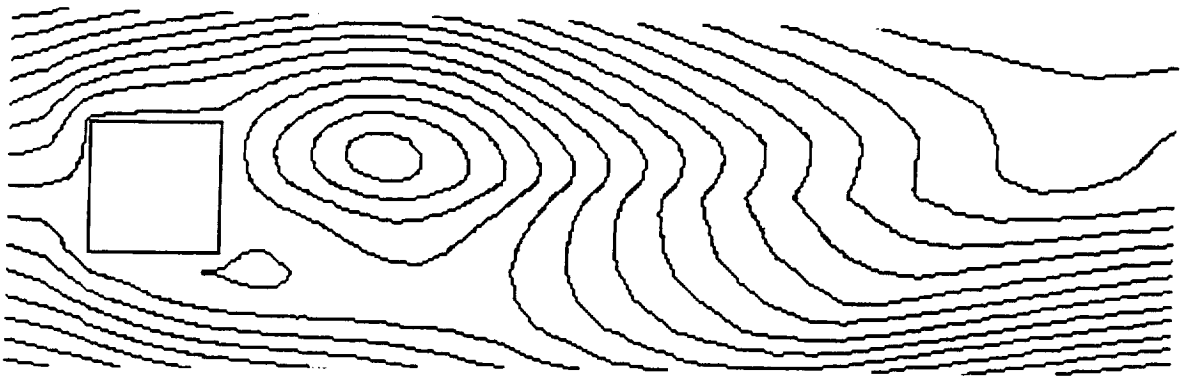

(b) $C_m = 0.01$

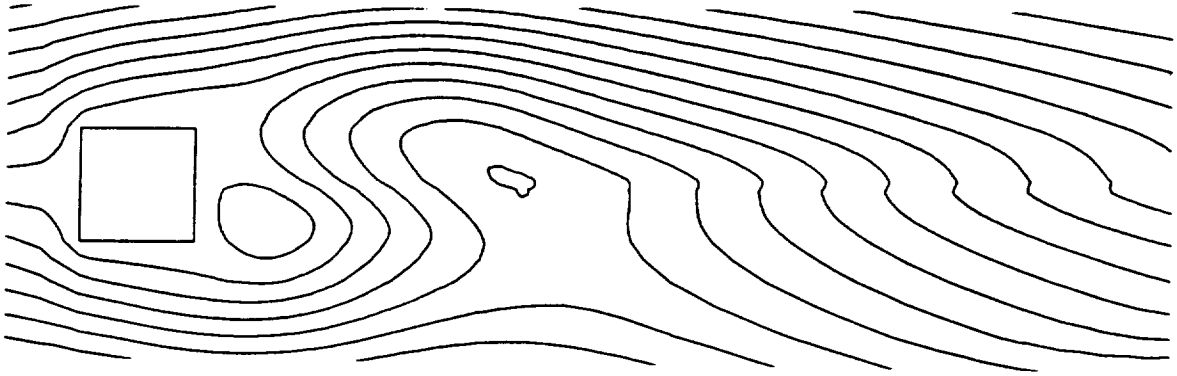

(c) $C_m = 0.02$

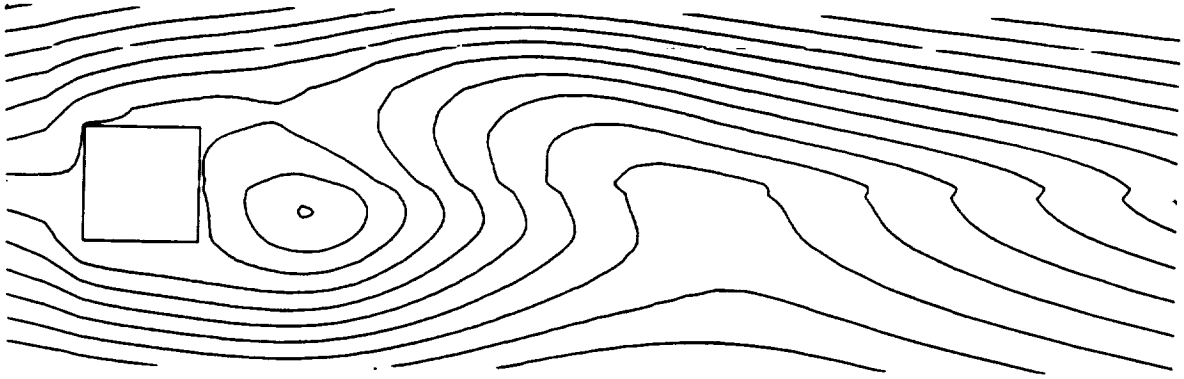

(d) $C_m = 0.05$

Fig. 3.25 Streamlines from steady computation ($Re = 1.25 \times 10^5$)

Chapter 4

CONCLUDING REMARKS

Numerical investigation of flow across rectangular cylinders is conducted with and without jets in the range of Reynolds numbers between 1 X 10^4 to 1.25 X 10^5. The Strouhal number, average base pressure coefficient, lift and drag coefficients are numerically estimated in the absence of jet. When jet is considered, possibility of drag reduction is examined. Drag coefficient decreases initially with an increase in jet momentum coefficient $C_{m,}$ but beyond a value of 0.01, C_d actually inceases.

REFERENCES

1 Roshko, A., 1954, "On the Drag and Shedding Frequency of Two-Dimensional Bluff Bodies," NACA Technical Note 3169, July 1954

2 Bostock, B. R., and Mair, W. A., 1972, "Pressure Distributions and Forces on Rectangular and D-shaped Cylinders," The Aeronautical Quarterly, Vol. 23 (part 1), February 1972, pp. 1-6.

3 Bearman, P. W., and Truman, D. M., 1972, "An Investigation of Flow around Rectangular Cylinders," The Aeronautical Quarterly, Vol. 23 (part 3), August 1972, pp. 229 -237.

4 Knauss, D. T., and John, J. E. A., 1976, "The Vortex Frequencies of Bluff Cylinders at Low Reynolds Numbers," Journal of Hydronautics, Vol. 10, No. 4, October 1976, pp. 121-126.

5 Atsushi, O.,1982, "Strouhal Numbers of Rectangular Cylinders," Journal of Fluid Mechanics, Vol. 123, October1982, pp. 379-398.

6 Clements, R. R., 1973, "An Inviscid Model of Two-Dimensional Vortex Shedding," Journal of Fluid Mechanics, Vol. 57(part2), February 1973, pp. 321-336.

7 Davis, R. W., and Moore, E. F., 1982, "A Numerical Study of Vortex Shedding from Rectangles," Journal of Fluid Mechanics, Vol. 116, March 1982, pp. 475-505.

8 Davis, R. W., Moore, E. F., and Purtell, L. P., 1984 "A Numerical-Experimental Study of Confined Flow around Rectangular Cylinders," Physics of Fluids, Vol. 27, No.1, January 1984, pp. 46-59.

9 Oh, S., and Roberts, L.,1989, "Control of Separated Flow Past a Cylinder Using Tangential Wall Jet Blowing," JIAA TR-93, Dept. of Aeronautics and Astronautics, Stanford University, July 1989

10 Atsuchi, S., Tiwari, S. N., and Kalburgi, V., 1998, "Investigation of Drag Reduction on a Two-Dimensional Circular Cylinder by Ejecting a Jet from the Rear Stagnation Region," AIAA Paper No. 98-0674, January 1998

11 Apselt, C. J., West, G. S., and Szewczyk, A. A., 1973, "The Effects of Wake Splitter Plates on the Flow Past a Circular Cylinder in the Range 10^4<R<5 X 10^4," Journal of Fluid Mechanics, Vol. 61, Part 1, October 1973, pp. 187-198

12 Fluent Inc., Fluent Code V.4.2 User Manual, Fluent Inc., Lebanon, NH, 1992.

13 Atsuchi, S., 1997, "Investigation of Drag Reduction on a Two-Dimensional Circular Cylinder by Ejecting a Jet from the Rear Stagnation Region," Master Thesis, Old Dominion University, Norfolk, VA, August 1997

14 Zukauskas, A., and Ziugzda, J., "Heat Transfer of a Cylinder in Crossflow," Hemisphere Publishing Corporation, New York, 1985